(1) Lee
(2) Murphy
(3) O'Neil

DNA TR-81-45

INFRARED PROGRAM SUPPORT

EXCEDE and Related Topics

Douglas H. Archer
Mission Research Corporation
P. O. Drawer 719
Santa Barbara, California 93102

30 November 1981

Final Report for Period 1 November 1980—30 November 1981

CONTRACT No. DNA 001-81-C-0081

APPROVED FOR PUBLIC RELEASE;
DISTRIBUTION UNLIMITED.

THIS WORK WAS SPONSORED BY THE DEFENSE NUCLEAR AGENCY
UNDER RDT&E RMSS CODE B322081466 S99QAXHI00002 H2590D.

Prepared for
Director
DEFENSE NUCLEAR AGENCY
Washington, DC 20305

Destroy this report when it is no longer needed. Do not return to sender.

PLEASE NOTIFY THE DEFENSE NUCLEAR AGENCY, ATTN: STTI, WASHINGTON, D.C. 20305, IF YOUR ADDRESS IS INCORRECT, IF YOU WISH TO BE DELETED FROM THE DISTRIBUTION LIST, OR IF THE ADDRESSEE IS NO LONGER EMPLOYED BY YOUR ORGANIZATION.

DNA PRINTING PLANT

UNCLASSIFIED

SECURITY CLASSIFICATION OF THIS PAGE *(When Data Entered)*

REPORT DOCUMENTATION PAGE		READ INSTRUCTIONS BEFORE COMPLETING FORM
1. REPORT NUMBER DNA-TR-81-45	2. GOVT ACCESSION NO.	3. RECIPIENT'S CATALOG NUMBER
4. TITLE *(and Subtitle)* INFRARED PROGRAM SUPPORTS EXCEDE and Related Topics		5. TYPE OF REPORT & PERIOD COVERED Final Report for Period 1 Nov 80 - 30 Nov 81 6. PERFORMING ORG. REPORT NUMBER MRC-R-675
7. AUTHOR(s) Douglas H. Archer		8. CONTRACT OR GRANT NUMBER(s) DNA 001-81-C-0081
9. PERFORMING ORGANIZATION NAME AND ADDRESS Mission Research Corporation 735 State Street, P.O. Drawer 719 Santa Barbara, California 93102		10. PROGRAM ELEMENT, PROJECT, TASK AREA & WORK UNIT NUMBERS Task S99QAXHI000-02
11. CONTROLLING OFFICE NAME AND ADDRESS Director Defense Nuclear Agency Washington, D.C. 20305		12. REPORT DATE 30 November 1981 13. NUMBER OF PAGES 90
14. MONITORING AGENCY NAME & ADDRESS*(if different from Controlling Office)*		15. SECURITY CLASS *(of this report)* UNCLASSIFIED 15a. DECLASSIFICATION/DOWNGRADING SCHEDULE N/A Since UNCLASSIFIED

16. DISTRIBUTION STATEMENT *(of this Report)*

Approved for public release, distribution unlimited.

17. DISTRIBUTION STATEMENT *(of the abstract entered in Block 20, if different from Report)*

18. SUPPLEMENTARY NOTES

This work was sponsored by the Defense Nuclear Agency under RDT&E RMSS Code B322081466 S99QAXHI00002 H2590D.

19. KEY WORDS *(Continue on reverse side if necessary and identify by block number)*

Electron Beams
Electron Deposition
EXCEDE
Infrared Radiation
Plasma Radiation

20. ABSTRACT *(Continue on reverse side if necessary and identify by block number)*

Further work, related to EXCEDE experiments, and to LWIR emission processes, is described. Efforts to account for the enhanced optical emission observed in the EXCEDE:SPECTRAL experiment on the basis of excitation by hot plasma electrons, using the independent particle deposition model, failed. The data appear consistent with a beam-plasma discharge mechanism. Analysis of ground-based photographic data imply that the region of enhancement extends for several hundred meters along

DD FORM 1 JAN 73 1473 EDITION OF 1 NOV 65 IS OBSOLETE

UNCLASSIFIED

SECURITY CLASSIFICATION OF THIS PAGE *(When Data Entered)*

20. Abstract (continued)

the earth's magnetic field.

Study of plasma radiation from electron-beam irradiated air leads to the conclusion that EXCEDE is not the optimum tool for verifying our IR models for bound-bound recombination radiation.

TABLE OF CONTENTS

TABLE OF CONTENTS (continued)

TABLE OF CONTENTS (concluded)

LIST OF ILLUSTRATIONS

LIST OF ILLUSTRATIONS (concluded)

LIST OF TABLES

SECTION 1
INTRODUCTION

In a continuing effort to provide support to the Defense Nuclear Agency (DNA) infrared (IR) program, particularly the field program, we have addressed several topics, delineated in the "work statement" to this contract, that may be summarized as follows.

1. Continue and complete studies being done in conjunction with AFGL, Photometrics, and TIC to determine the validity of our electron beam deposition code by detailed comparison with EXCEDE:SPECTRAL optical data.

2. Continue and complete studies to determine the spatial distribution of infrared plasma radiation from electron beam-irradiated air, and the magnitude of competing molecular band radiation. Use the results to determine the feasibility of using an EXCEDE-type experiment to check the validity of the theoretical model of plasma radiation.

3. Provide a better estimate of the importance of N_2O as an LWIR radiator in a nuclear environment by determining and utilizing better input data on its formation process through the reaction $N_2(A^3\Sigma) + O_2 \rightarrow N_2O + O$, and by attempting to determine the excitation rate of its fundamental bands by sunlight absorption.

4. Attempt to determine realistic rates for photon scatter excitation of uranium oxide and fission fragment oxide ions with the object of providing better estimates of the importance of these species as LWIR radiators in a nuclear environment.

5. By utilizing prior MHD multiburst calculations, make a preliminary assessment of the degree to which our conclusions regarding the relative importance of LWIR radiators in a single-burst environment are modified in a multiburst environment.

Item 1, treated in Section 2, involves an attempt to define the spatial dimensions of the anomalously bright region surrounding the EXCEDE: SPECTRAL electron guns, and to determine if the single particle deposition model can possibly account for the anomaly. The usefulness of the EXCEDE concept as a diagnostic tool for verifying our IR nuclear-predictive models is vitally dependent on our ability to understand the mechanisms involved.

Item 2, treated in Section 3, involves a study, based on ARCTIC code calculations, of plasma radiation excited by a high-current beam of 3-keV electrons. The main purpose of this work is to see if the bound-bound component of IR plasma radiation in an electron beam experiment, such as EXCEDE, is likely to be intense enough, relative to other competing emissions, to permit an experimental check on the validity of our theoretical models for this radiation.

Items 3, 4, and 5, treated in Section 4, deal with questions that arose in an earlier study (Reference 1-1) of the relative importance of various long wavelength infrared (LWIR) radiators in a nuclear environment.

A summary of our conclusions is presented in Section 5.

SECTION 2

ANOMALOUS BRIGHTENING IN THE EXCEDE: SPECTRAL EXPERIMENT

PRELIMINARY

This section represents a continuation of the work reported in Section 3 of Reference 2-1. It is suggested that the reader become acquainted with the details of that section before proceeding. A brief summary is as follows.

In order to interpret optical/IR data from electron-impact excited regions of the atmosphere (e.g. aurora, EXCEDE) in terms of a nuclear environment, the tacit assumption has been that the deposition mechanism is similar to that for X-ray photoelectrons, or fission beta electrons. That is, the assumption has been that the electrons deposit their energy essentially independently so that collective effects, that may give rise to internal electric fields, are negligible.* In such cases, given the proper set of cross sections, the electron energy spectrum can be computed, the optical/IR radiation predicted, and our nuclear-IR models checked for accuracy. If, on the other hand, the electrons in a field experiment should deposit their energy quite differently, because of collective effects, then their energy spectrum is likely to differ from that arising as a result of independent particle deposition, as are also the relative efficiencies for production of various optical and infrared radiations. Inferences drawn regarding the IR models used for application to the nuclear (independent particle) case may then be erroneous.

---

* The appropriateness of this assumption for the auroral and nuclear environments is treated in a later subsection.

In order to check the applicability of the independent particle model to EXCEDE experiments, we used a computer code, that incorporates such a model, to calculate the energy deposition rate surrounding electron beams in the atmosphere. Applying a fluorescence efficiency factor of 4.5×10^{-3} for N_2^+1 Neg. (3914 Å) emission,* we then compared the results with photographic data from the PRECEDE II and EXCEDE:SPECTRAL events. The results of those comparisons were reported in Reference 2-1.

Briefly, the PRECEDE II comparisons were somewhat inconclusive because absolute intensities are not available from the field data. However, the EXCEDE:SPECTRAL data are greatly at odds with the code calculations and seem to imply that the independent particle model is woefully inadequate to account for the observations, especially in a region within a few tens of meters of the electron accelerator. In this region, the measured 3914 Å brightness, which is proportional to the energy deposition rate, is up to two orders-of-magnitude larger than the calculated values.

Several questions immediately arise. For example: What is the mechanism that produces the anomalous brightening? Does it involve collective effects that may render interpretation of optical/IR data questionable? Over what region does the anomaly pertain? Is there a region sufficiently far from the accelerator where the deposition behaves "normally?" Is the N_2^+ First Negative (3914 Å) fluorescence efficiency inferred from auroral data, and measured under low-current conditions in the laboratory, inapplicable under the high-current conditions of EXCEDE? Answers to most of these questions are not known for certain at the present time, although we will attempt to address some of them in this section.

---

* This factor is consistent with auroral data and with many laboratory experiments involving low-current (usually in the tens of μa range) electron beams (Reference 2-2).

Possible mechanisms that have been suggested include various discharge phenomena, particularly the so-called "beam plasma discharge" (BPD) observed in laboratory experiments (References 2-3 to 2-6), return currents induced by vehicle charging, and payload outgassing. The latter mechanism, however, probably plays a relatively minor role since the anomaly is present even at altitudes as low as 80 km where the ambient density is believed to be considerably greater than that from outgassing. At present, some discharge phenomenon appears to be favored.

If, in fact, a BPD is actually responsible, it is noteworthy that vacuum tank experiments (Reference 2-7) have shown that the electron energy spectrum is then dramatically changed, with electron energies greater than the incident beam energy present along with a greatly enhanced low energy tail. As mentioned above, one would then have to view any extrapolation of optical/IR data therefrom to the nuclear case with considerable suspicion. Alternatively, validation of our optical/IR models could still be accomplished provided we knew the electron energy spectrum throughout the dosed region. However, this would require detailed, and probably difficult, measurements which should be avoided if at all possible.

For interpretation of the EXCEDE:SPECTRAL data, and particularly for use in planning any future EXCEDE experiment, we would especially like to know: (1) the extent of the anomalous region, and (2) whether or not the electron energy spectrum in this region differs significantly from that predicted on the basis of independent particle deposition. Closely related to Item 2 is the question whether, under high-current conditions, the effective fluorescence efficiency for 3914 Å emission can be raised to the point where the observations can still be accounted for on the basis of independent particle theory. This section addresses these two topics.

FURTHER COMPARISONS WITH FIELD DATA

As in Reference 2-1, Section 3, the data and calculations discussed here all pertain to an electron pulse initiated at an altitude of about 123 km on rocket ascent during the EXCEDE:SPECTRAL event.

On Size of Anomalous Region

The best hope of estimating the size of the enhanced region comes from a study of the ground-based photographic data taken by Technology International Corporation (TIC). Figure 3-9 of Reference 2-1 shows a comparison between the relative radiance values measured by TIC, as a function of distance along the beam, and our code calculations for 3914 Å. In that figure we had arbitrarily normalized the TIC data to correspond to the calculated curve at a point 3 km along the beam from the accelerator. Actually, however, the figure is not particularly meaningful for two reasons. First, because an absolute intensity calibration for the data was not available at that time and, second, because the spatial resolution of the data is estimated to be in the range from about 20 to 50 meters (Reference 2-8), whereas the theoretical curve corresponds to infinitely sharp (0 meter) spatial resolution.

A somewhat more meaningful comparison is shown below in Figure 2-1. Here, the preliminary values of absolute intensity measured by TIC (Reference 2-8 are compared with four different theoretical curves corresponding to spatial resolutions of 0, 10, 20, and 30 meters. Since the resolution of the camera data is believed to exceed 20 meters, the lowest of the (solid) theoretical curves is probably the most appropriate for comparison purposes. Nevertheless, there is still a certain degree of uncertainty in making this comparison, partly because of the resolution question, and partly because the theoretical curves refer to radiance in just the 3914 Å (N_2^+ 1 Neg.) band whereas the photographic data include other wavelengths as well.

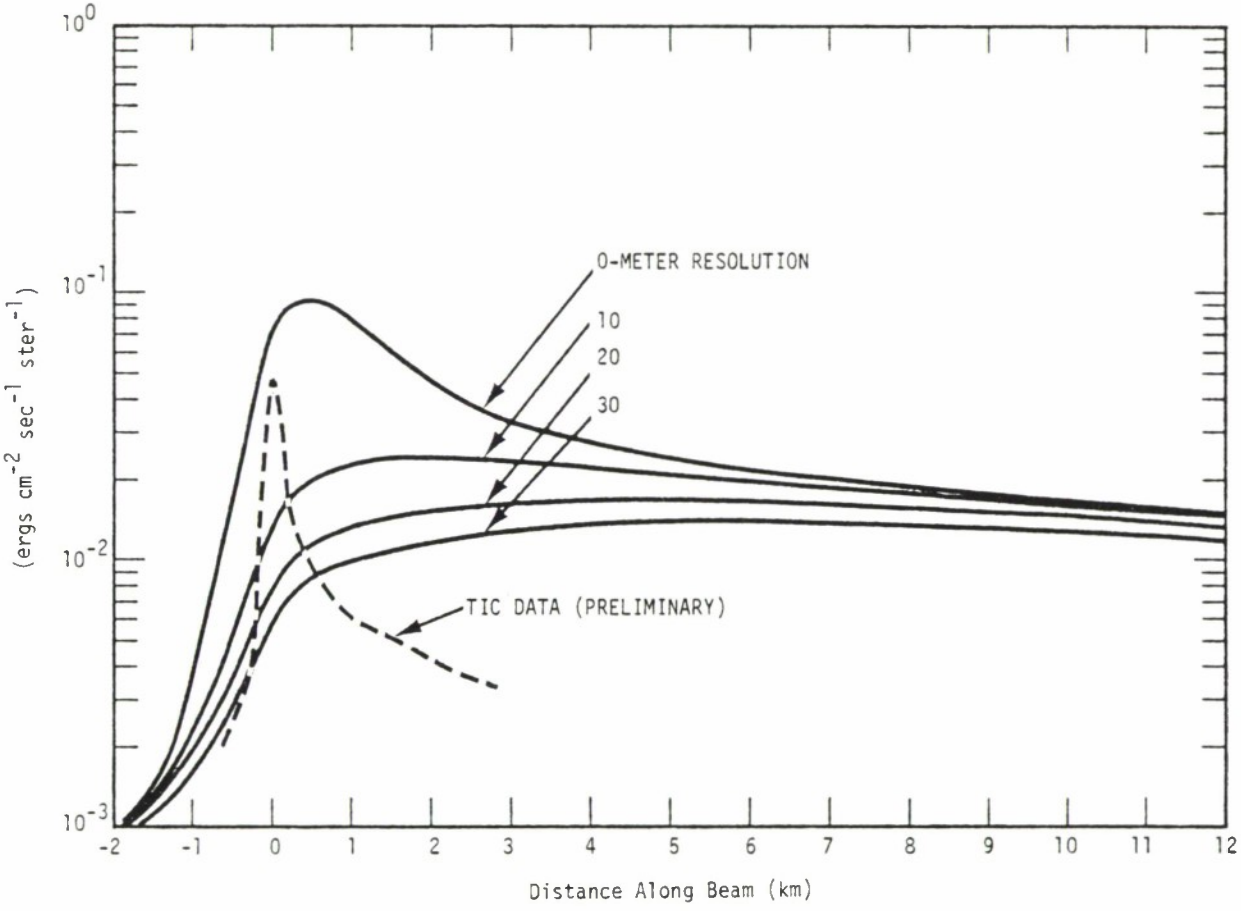

Figure 2-1. EXCEDE:SPECTRAL radiance (3914Å) normal to beam axis at 123 km; calculations and photographic data compared.

Thus, to compare the data and calculations on an equal basis, the data curve (dashed) should be lowered by some factor, estimated to be about 1.5.

A still more meaningful comparison can be made on the basis of the crosswise integrated intensity as a function of distance along the beam. This has the advantage of removing the dependence of the results on the spatial resolution of the observing equipment. The crosswise integrated intensity, T(Z), can be defined as the integrated intensity along a line normal to the beam at a distance Z from the accelerator. That is, if I(Z,R) is the intensity normal to the beam at a distance Z along the axis from the accelerator, and at a radial distance R from the axis, then

$$T(Z) \equiv \int_{-\infty}^{\infty} I(Z,R)dR \quad . \qquad (2\text{-}1)$$

Thus, given a set of radial intensity distributions, I(Z,R), at various distances along the beam from the accelerator, the area under each gives the crosswise integrated intensity.

Figure 2-2 shows the calculated (lower solid curve) and observed (dashed curve) radial intensity distributions at a distance of 4 meters along the beam from the gun. The data were taken by Photometrics (Reference 2-8) using a rocket-borne black and white camera whose filter band extends from about 3600 Å to 4700 Å. However, since the calculated curve is for the 3914 Å band only, the dashed curve should be lowered by some factor, estimated to be about 1.5 (Reference (2-10). Even so, it is clear that the area under the dashed curve (crosswise integrated intensity) is considerably greater than that under the theoretical curve. The upper solid curve in Figure 2-2 is the calculated intensity distribution increased by a factor of 10 and shifted to the left to bring its peak into line with the camera data. More will be said about that in a later subsection.

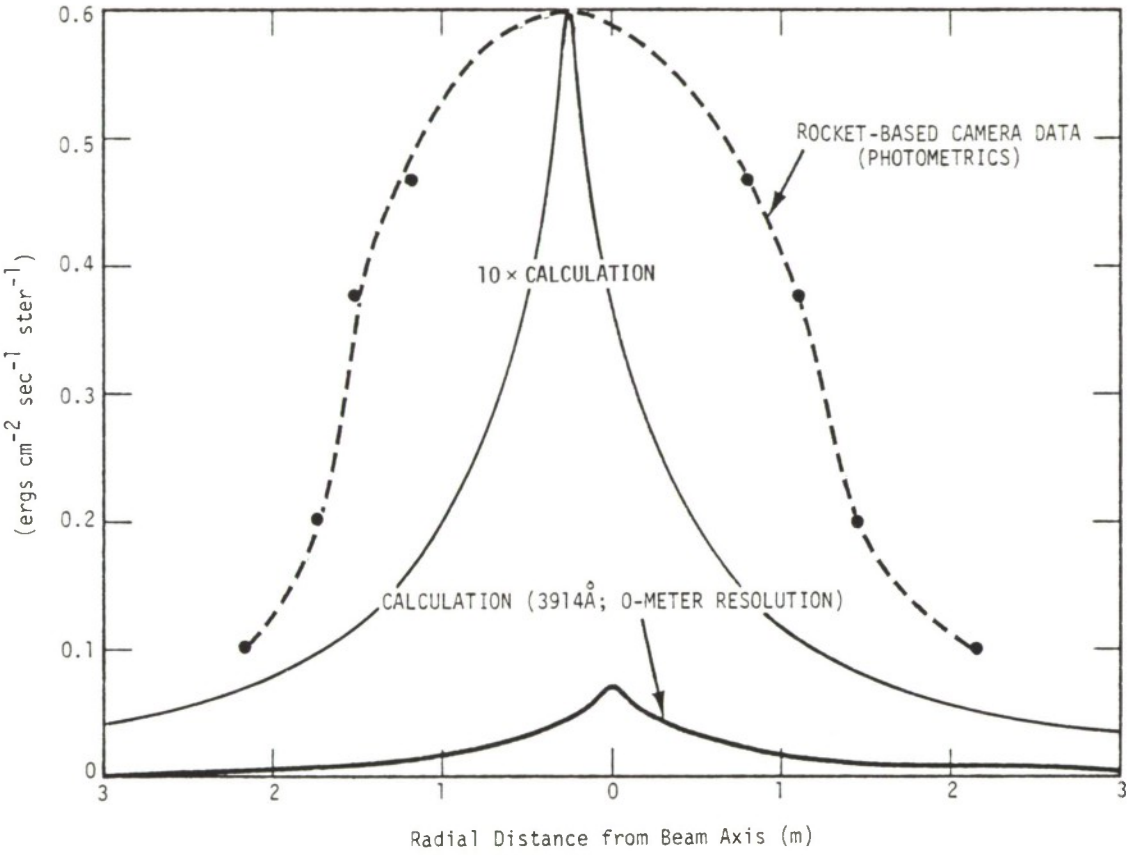

Figure 2-2. Radial intensity distribution at + 4.0 meters from EXCEDE: SPECTRAL gun (123-km altitude).

Figures 2-3 to 2-5 are examples of similar comparisons between the calculated and observed radial intensity distributions at distances along the beam from the gun of 44, 324, and 1450 meters, respectively. In these figures the data are from the ground-based photographic image recorded by TIC (Reference 2-11). Again, as mentioned above, since the data includes all wavelengths for which the camera film was sensitive, the dashed curves should be lowered by some factor ($\approx$1.5). Nevertheless, a visual inspection of Figures 2-3 to 2-5 shows that the area under the observed intensity distribution (crosswise integrated intensity) is greater than than under the theoretical distribution at 44 meters from the gun (Figure 2-3), that the reverse is true at 1450 meters (Figure 2-5), and that the two areas are equal at some intermediate distance.

The crosswise integrated intensity, defined by Equation 2-1, can be defined, alternatively, (for an optically thin medium) in terms of the volume emission rate at 3914 Å, $\dot{\varepsilon}_{3914}$, by the expression

$$T_{3914}(Z) = \int_0^\infty 2\pi R \dot{\varepsilon}_{3914}(Z,R)\,dR \qquad (2\text{-}2)$$

or, in terms of the volume deposition rate, $\dot{\varepsilon}(Z,R)$, in normalized units of eV gm^{-1} (See Reference 2-1), by the expression

$$T_{3914}(Z) = 2.25 \times 10^8 I\rho \int_0^\infty R\dot{\varepsilon}(Z,R)\,dR \quad (\text{ergs cm}^{-1}\ \text{sec}^{-1}\ \text{ster}^{-1}) \quad . \qquad (2\text{-}3)$$

In Equation 2-3, I is the beam current in amperes, ρ is the local atmospheric density (gm cm^{-3}) and the radial distance, R, is measured in meters.

Equations 2-2 and 2-3 were used, together with values for $\dot{\varepsilon}(Z,R)$ computed by our deposition code (see Reference 2-1, Figure 3-3), to calculate the crosswise integrated intensity as a function of distance along the beam. The results are shown in Figures 2-6 and 2-7. Figure 2-6 gives the results in normalized units for a single 3-keV electron whereas Figure 2-7

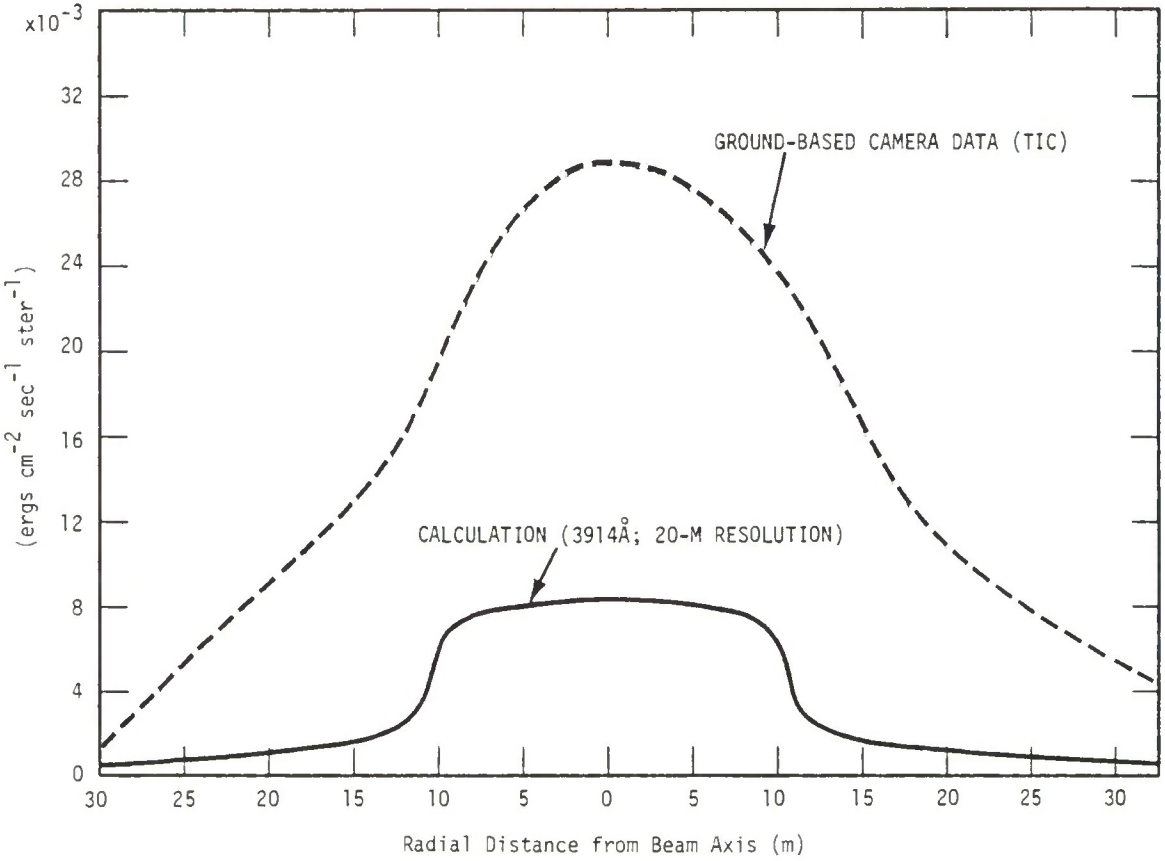

Figure 2-3. Radial intensity distribution at + 44 meters from EXCEDE: SPECTRAL gun (123-km altitude).

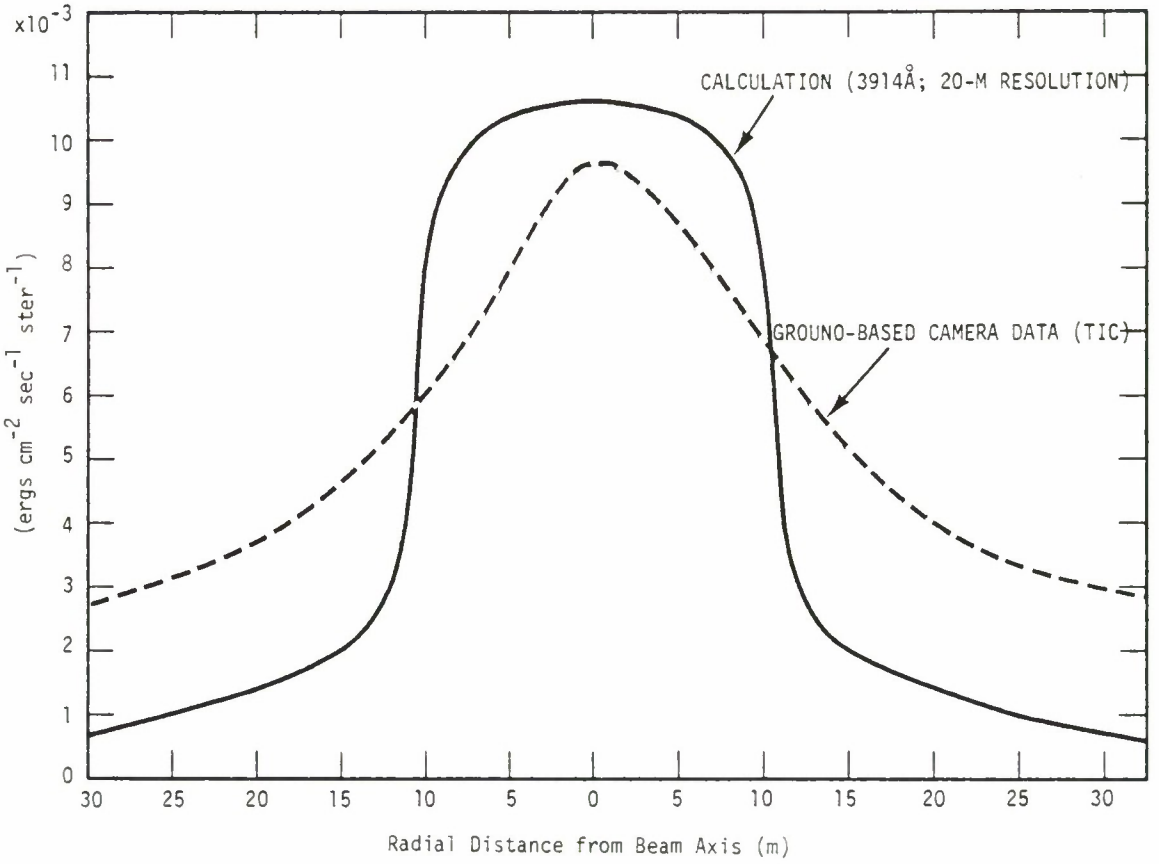

Figure 2-4. Radial intensity distribution at 324 meters from EXCEDE: SPECTRAL gun (123-km altitude).

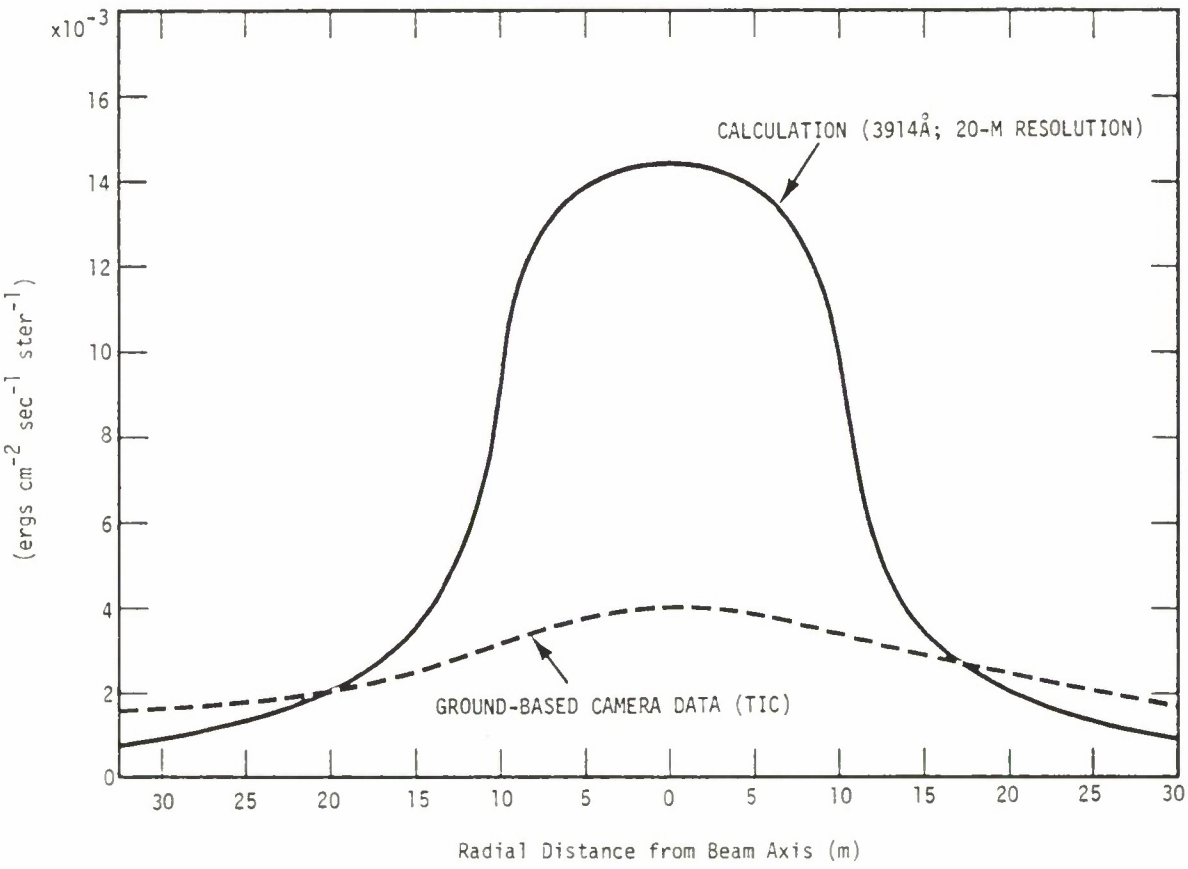

Figure 2-5. Radial intensity distribution at + 1450 meters from EXCEDE: SPECTRAL gun (123-km altitude).

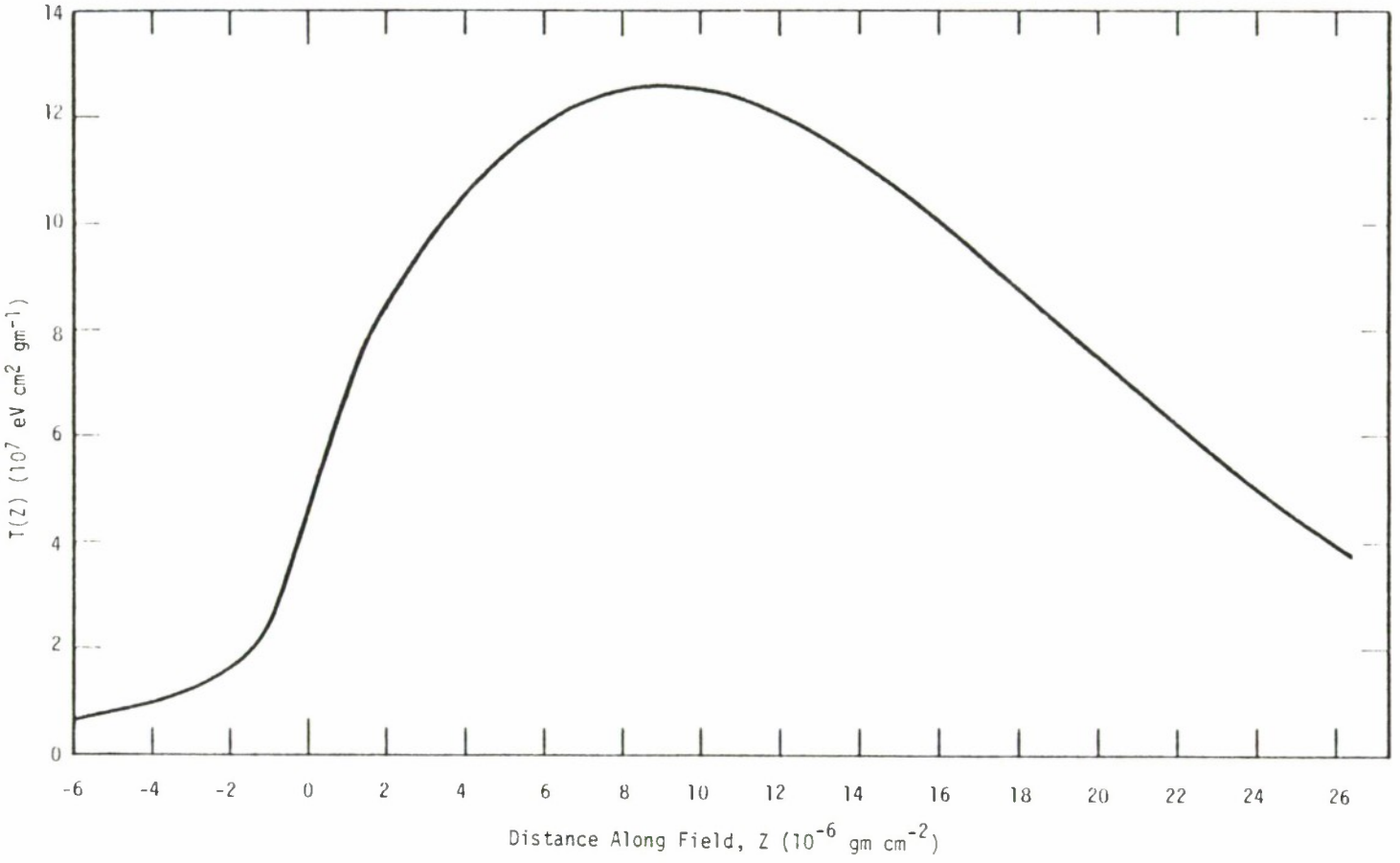

Figure 2-6. Calculated crosswise integrated intensity, T(Z), in magnetic field of 0.5 gauss in normalized units for unit number current exiting gun in 30° cone with axis parallel to $\vec{B}$ (E_o = 3 keV).

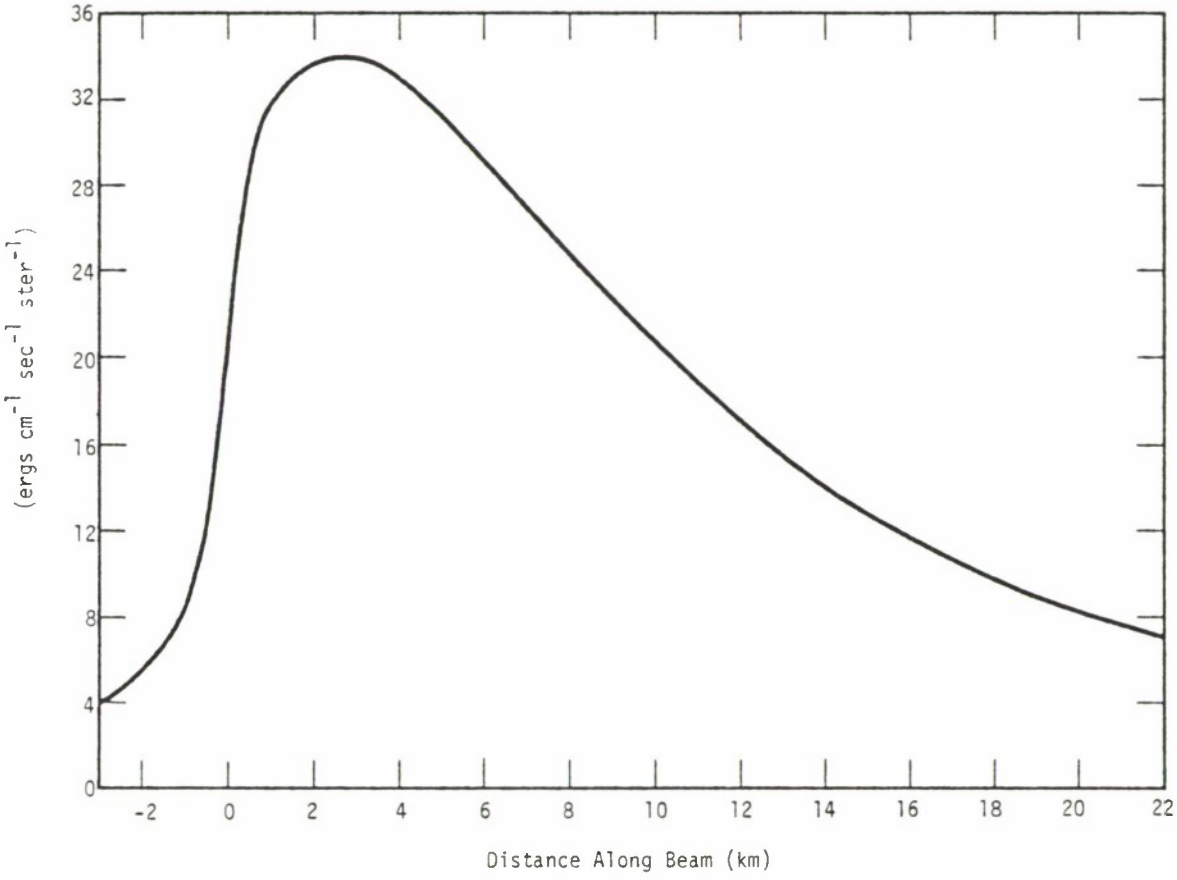

Figure 2-7. Calculated crosswise integrated intensity (3914Å) at 123 km for 7 amp, 3 keV beam exiting gun in 30° cone with axis parallel to $\vec{B}$.

shows the results for the particular case of interest here, namely a 7 amp beam at 123-km altitude. In both figures the electron gun is located at the origin, and emission for negative values of the distance arises from backscattered electrons.

Figure 2-8 compares the calculated crosswise integrated intensity (solid curve) with that observed (dashed curve). The observed values were obtained by finding the areas under the radial intensity distributions provided by TIC. For this purpose, we arbitrarily extrapolated the wings of the distributions to zero intensity.* A value for T(Z), inferred from the Photometrics data (Figure 2-2) for a distance of 4 meters forward of the gun, is also shown in Figure 2-8.

A comparison of the two curves shown in Figure 2-8 provides some measure of the extent of the enhanced region. From the points of intersection of the dashed and solid curves, we infer that the enhancement extends from about 280 m behind the gun to about 800 m in front of it. These values, however, must be changed somewhat if we allow for the fact that the dashed curve should be lowered by some factor, as mentioned above, because it represents emission over a broader band than just the 3914 Å band represented by the theoretical curve. For example, if we assume the factor is 1.5, the enhancement then extends from about 200 m behind to about 550 m in front of the gun. If the factor is 2.0, it extends from about 130 m behind to about 350 m in front.

Further considerations, introduced in the following subsection, lead to the conclusion that the extent of the enhanced region, as inferred from the TIC data, is even less precisely defined than the foregoing numbers suggest.

---

* The implication of these extrapolations to the accuracy of the results is discussed in the next subsection.

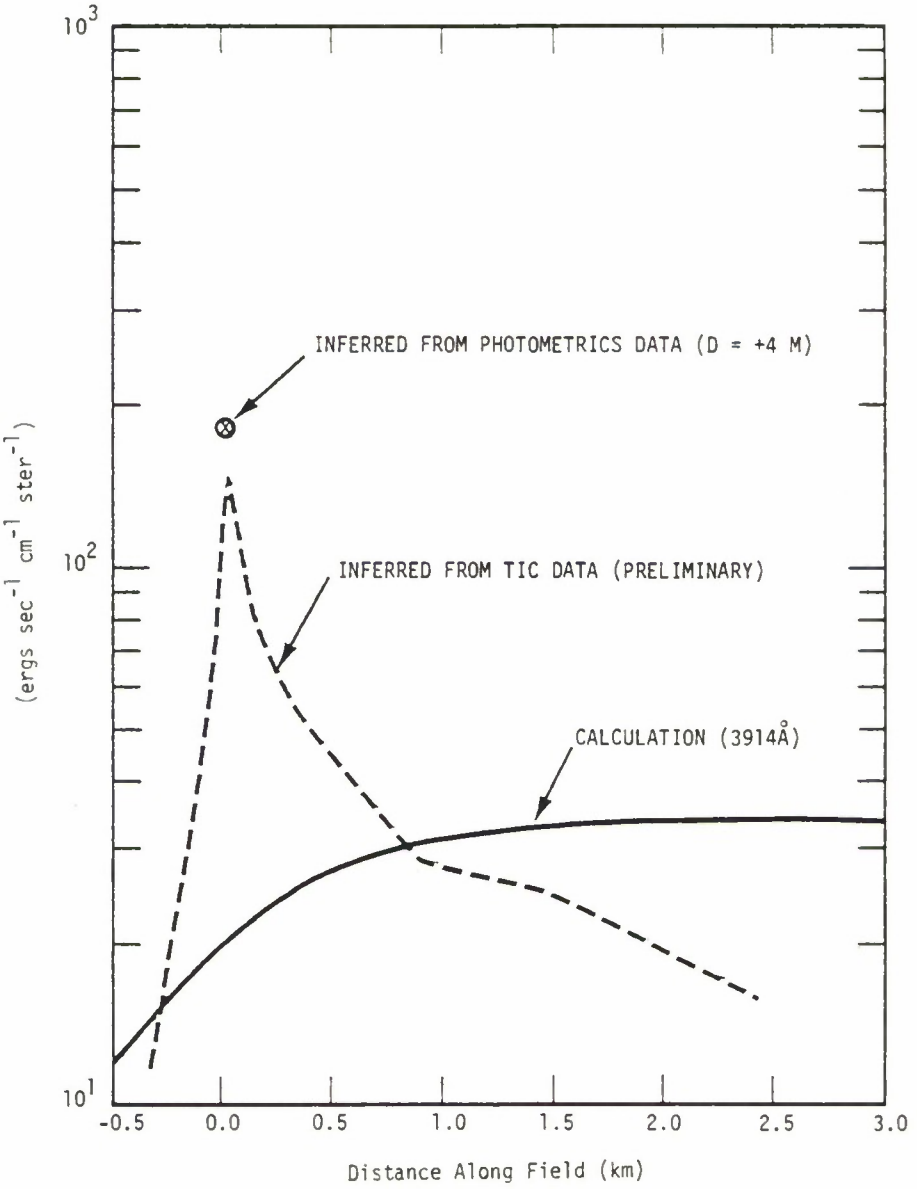

Figure 2-8. Crosswise integrated intensity at 123-km altitude (EXCEDE:SPECTRAL).

On Energy Conservation and Accuracy of Above Results

In Figure 2-6 we showed the calculated crosswise integrated intensity, in normalized units, for a current of 1 (3 keV) electron sec^{-1} exiting the gun in a 30° cone with axis parallel to the earth's magnetic field. The area under this curve (extended from $-\infty$ to $+\infty$) equals 3 keV. However, for a magnetic dip angle of 77° (Poker Flat, Alaska), the column density of air along the earth's field above an altitude of 123 km is about 23×10^{-6} gm cm^{-2}. Thus, in Figure 2-6, the energy represented by that portion of the curve for which $Z > 23 \times 10^{-6}$ gm cm^{-2} would escape from the atmosphere. From the respective areas involved, we find, on the basis of the independent particle model, that about 8 percent of the energy should escape the atmosphere.

Turning now to the actual EXCEDE:SPECTRAL observations, it is of interest to see how the power, inferred from the area under the dashed curve in Figure 2-8, compares with the total power in the EXCEDE beam. For this purpose, we have arbitrarily extrapolated the dashed curve to zero in both wings, measured its area, and multiplied by 4π. The result is 1.43×10^{8} ergs sec^{-1} in the photographic band. If we assume that the photographic film was sensitive to 50 percent more energy than represented by just the 3914 Å band, and that the fluorescence efficiency of the 3914 Å band is 4.5×10^{-3}, then the total power represented by the TIC data, is

$$P_{TIC} = 1.43 \times 10^{8} / (1.5 \times 4.5 \times 10^{-3}) = 2.1 \times 10^{10} \text{ (ergs sec}^{-1}\text{)} \quad (2\text{-}4)$$

But the power in the electron beam is

$$\begin{aligned} P_{beam} &= (\text{electrons/sec-amp}) \times (\text{amps}) \times (\text{eV/electron}) \times (\text{ergs/eV}) \\ &= (6.25 \times 10^{18}) \times (7) \times (3 \times 10^{3}) \times (1.6 \times 10^{-12}) \\ &= 2.1 \times 10^{11} \text{ (ergs sec}^{-1}\text{)} \quad . \end{aligned} \quad (2\text{-}5)$$

Therefore, the TIC data seem to account for only 10 percent of the beam energy. Where has the rest of it gone?

For one thing part of it, but probably no more than about 8 percent as indicated above, escaped the atmosphere.* However, most of the missing energy, we believe, is lost in the film fog. That is, it was deposited in large volumes of air outside the periphery of the visible image such that the irradiancy at the camera, from those regions, was below the film threshold.

This raises a question concerning the accuracy of our determination of the crosswise integrated intensity from the measured radial intensity distributions. This is because the wings of the measured curves (see dashed curves in Figures 2-3 to 2-5) are below film threshold and we can only guess how they fall off at larger radial distances. In obtaining the dashed curve in Figure 2-8, we used a linear extrapolation of the wings to zero intensity for each of the measured radial distributions. More likely the intensity in the wings falls off less rapidly, as it does in our independent particle model, with the result that each point in the dashed curve of Figure 2-8 should be raised by some unknown factor. Similarly, for the purpose of measuring the area under the dashed curve in Figure 2-8, we linearly extrapolated the two ends to zero. They, too, probably fall off less rapidly with distance.

The conclusion then is, that in order to conserve energy, the dashed curve in Figure 2-8 needs to be raised by some unknown amount, and tails added that extend to great distances in both forward and backward directions. It is not possible, however, from the photographic data, to

---

* One would expect that since an abnormally large fraction of the energy is deposited near the electron gun, a smaller than normal fraction would be available to escape.

quantify these changes. All we can say regarding the dashed curve in Figure 2-8 is that it should probably be raised. With reference to the preceding subsection, this means that we cannot be at all precise about the spatial dimensions of the anomalous region surrounding the accelerator, other than to say that it appears to extend for several hundred meters along the magnetic field.

HOT PLASMA EXCITATION OF 3914 Å

In the preliminary discussion of this section, we mentioned several mechanisms that have been suggested as possible candidates to explain the anomalous enhancement of emission observed in the EXCEDE:SPECTRAL experiment. Favored among these mechanisms is some discharge phenomenon, possibly the "beam plasma discharge" (BPD) that has been studied rather extensively in the laboratory. It was also mentioned that the latter mechanism results in an electron energy spectrum that deviates markedly from what one expects from electron energy deposition in the aurora, or following a nuclear detonation, for which the independent particle model should be a very good approximation. Since the efficiency for production of certain optical and IR bands may be sensitive to the electron energy spectrum, use of optical/IR data from discharge-excited air to validate our nuclear-IR models may be hazardous. Of course, given the electron energy spectrum we can use codes, such as ARCTIC, to predict the optical/IR radiation for comparison with the data, and thereby check the models. But, "given the electron energy spectrum" means measuring it throughout the dosed region, which is a difficult and probably expensive thing to do. Therefore, insofar as EXCEDE is to be considered a viable tool for helping to validate our nuclear-IR codes, it would be of great benefit if it could be shown that the observed enhancement can be explained on the basis of independent particle deposition. Partly toward that end, the work in this subsection was undertaken.

The only way we can think of whereby the independent particle model might be able to account for the anomalous brightening is if the effective fluorescence efficiency for 3914 Å radiation is greatly increased by the presence of plasma electrons that have been heated by collisions with beam electrons to the point where they can produce further ionization and electronic excitation. The fluorescence efficiency for 3914 Å that we have used in our calculations, reported in Reference 2-1 and earlier in this section, is based on the results of numerous laboratory measurements (see, for example, the references given in Reference 2-12) as well as inferences from auroral data. However, as far as we can determine, in all of those experiments the current of electrons involved was too small to create a plasma hot enough to produce significantly more ionization. Therefore, to our knowledge, no experiment or calculation has previously been done to determine how plasma heating by a high-current (amperes) electron beam in air might act to modify the effective fluorescence efficiency.

To investigate this, we have made use of the ARCTIC code. This code was originally constructed by MRC, partly under DNA auspices, for use in analyzing and interpreting optical/IR data from the auroral ICECAP experiments. Details of the code, for auroral use, can be found in References 2-13 through 2-16, and a very brief summary is given in the following subsection. For use under high-current conditions, however, we found it necessary to make extensive changes in the code. A detailed description of these changes is presented in Appendix A, and a brief summary is given immediately following the next subsection. The changes, that include the introduction of additional cooling mechanisms, were necessary not only for the investigations of this section but also for the study of plasma radiation in EXCEDE experiments, described in Section 3.

Summary of Auroral Code "ARCTIC"

ARCTIC is a general purpose atmospheric electron deposition and chemistry code originally used to study the effects of a flux of auroral electrons upon the atmosphere. It calculates the electron energy deposition and partition, the subsequent atmospheric chemistry, optical and IR emissions, and electron heating effects.

Specifically, we can input a spectral flux of primary electrons with a given pitch-angle distribution and a specified magnetic dip angle. The electrons then interact with the atmosphere, consisting of N_2, O_2, O, CO_2, N, and an ambient electron gas. The code computes a number of items, as a function of altitude, including the secondary electron production rate spectrum, secondary flux spectrum, and the volume production rates of excited states by both the primaries and by all generations of secondary electrons.

The production rates of allowed states, i.e., the non-metastables, are then used, with allowance for branching and cascade, to compute directly the volume emission rates in various allowed lines and bands. The production rates of metastable states and the electron gas heating rate, computed in the deposition routine, are then fed into the chemistry subroutine where the species concentrations and electron and N_2 vibrational temperatures are calculated. These quantities are then used to compute the volume emission rates of radiation — both optical and IR — resulting from forbidden transitions and also from vibraluminescent and chemiluminescent reactions. These emission rates are output as functions of altitude and time.

In particular, the code provides for the excitation by the bombarding flux of 210 states (including $N_2(v=0\rightarrow7)$) among the species N_2, N_2^+, N, N^+, O_2, O_2^+, O, O^+, CO_2, and CO_2^+, while the chemistry subroutine treats over 200 reactions among 31 chemical species whose concentrations

are determined by integration of the rate equations using a combination Runge-Kutta and quasi-analytic approach. For determination of the electron temperature, the code includes direct heating by the bombarding electron flux and cooling by excitation of the metastable states of O, O^+, and N, rotational and vibrational excitation of N_2 and O_2, fine structure excitation of $O(^3P)$, and elastic collisions with N_2, O_2, O, and positive ions.

Volume emission rates output from the code include the following bands. From direct excitation of allowed states: the N_2^+ First Negative and Meinel bands, the N_2 Second Positive, O_2^+ First Negative, and certain IR bands of CO_2. From the species carried in the chemistry code: NO and NO^+ chemiluminescence in the fundamental and first overtone bands, CO_2 vibraluminescence in various IR bands, forbidden line radiation from O, O^+, N, and N^+, and bands of the O_2 atmospheric and infrared atmospheric systems. Full provision for the effects of quenching are included.

Summary of ARCTIC Code Changes Required Under High-Current Conditions

Under high-current conditions, we expect the electron temperature to attain values much higher than those in the aurora. It then becomes necessary to allow for cooling of the plasma electrons by other processes including excitation of some of the higher-lying electronic states, and even ionization of the major species. Furthermore, while attempting to run the code under EXCEDE-bombardment conditions, we found that certain cooling rate expressions, valid under auroral conditions, were invalid at higher electron temperatures. This necessitated, in those cases, drastic revision of the rates. The details of these and other changes that have been made are described in Appendix A. A brief summary is as follows.

- Additions to ARCTIC Code
  - Electron cooling by electronic excitation and ionization of 24 additional states of N_2, O_2, O.
  - Emission of 3914 Å photons through the processes:
    - $e_p + N_2(X^1\Sigma) \rightarrow 2\ e_p + N_2^+(B^2\Sigma)$

      $N_2^+(X^2\Sigma) + h\nu(3914\ \text{Å})$
    - $e_p + N_2^+(X^2\Sigma) \rightarrow e_p + N_2^+(B^2\Sigma)$

      $\rightarrow N_2^+(X^2\Sigma) + h\nu(3914\ \text{Å})$

    where e_p represents a plasma electron.
  - Ionization of $N_2(v>0)$
  - Ionization of $O_2(a^1\Delta)$ and $O_2(b^1\Sigma)$
  - Radiative-collisional recombination
- Changes in ARCTIC Code Models
  - Electron cooling by elastic scattering from N_2, O_2, O
  - Electron cooling by vibrational excitation of N_2, O_2.

Code Calculations and Results

After making the required changes and additions to the ARCTIC code, we exercised it under input conditions approximately simulating those in the EXCEDE:SPECTRAL experiment at an altitude of 123 km. The volume deposition rate was taken to be 1.48×10^{12} eV cm^{-3} sec^{-1}, which equals the maximum value calculated (using the independent particle model) for a 7 amp, 3 kV beam at 123-km altitude (see Reference 2-1, Figure 3-3). The code was run, under full bombardment conditions, for times to 10 sec.

The code output is voluminous. It includes production rates for over 200 states as well as the time dependence of more than 30 species concentrations, the electron temperature, and numerous optical/IR volume emission rates. Figure 2-9 shows only that part of the output that is especially relevant to this discussion. Included is the electron temperature and four different contributions to the volume emission rate of 3914 Å for times from 10^{-4} sec to 10 sec. These contributions, shown by curves 2, 3, 4, and 5 in Figure 2-9, arise from, respectively, (a) direct bombardment of N_2 by beam electrons, (b) direct bombardment of N_2^+ by beam electrons, (c) excitation of N_2 by hot plasma electrons, and (d) excitation of N_2^+ by hot plasma electrons. The dashed line 1, corresponding to 2.07×10^9 photons cm^{-3} sec^{-1}, is based on a fluorescence efficiency for the 3914 Å band of 4.5×10^{-3}, which is the value used in our comparisons with the EXCEDE:SPECTRAL photographic data.

Process (b), excitation of 3914 Å by bombardment of N_2^+ by beam electrons, is not actually in the ARCTIC code. We have estimated its effect (curve 3 in Figure 2-9) by noting that the cross section for the process is approximately 8.9 times that for the process $e_{beam} + N(^4S) \rightarrow e_{beam} + N(^2P)$, which is in the code. Thus, the volume production rate, $P(N_2^+(B)$, of the parent state of the N_2^+ First Negative system, by electron-beam bombardment, can be written as

$$P(N_2^+(B))_{\text{beam on } N_2^+} \approx 8.9\ p(N(^2P))[N_2^+] \qquad (2\text{-}6)$$

where $p(N(^2P))$ is the production rate of $N(^2P)$ atoms per $N(^4S)$ atom. But, from Reference 2-12, the volume emission rate, $\dot{\phi}_{3914}$, of the (0, 0) band (3914 Å) of the N_2^+ First Negative system is given by

$$\dot{\phi}_{3914} \approx 0.65\ P(N_2^+(B)) \quad . \qquad (2\text{-}7)$$

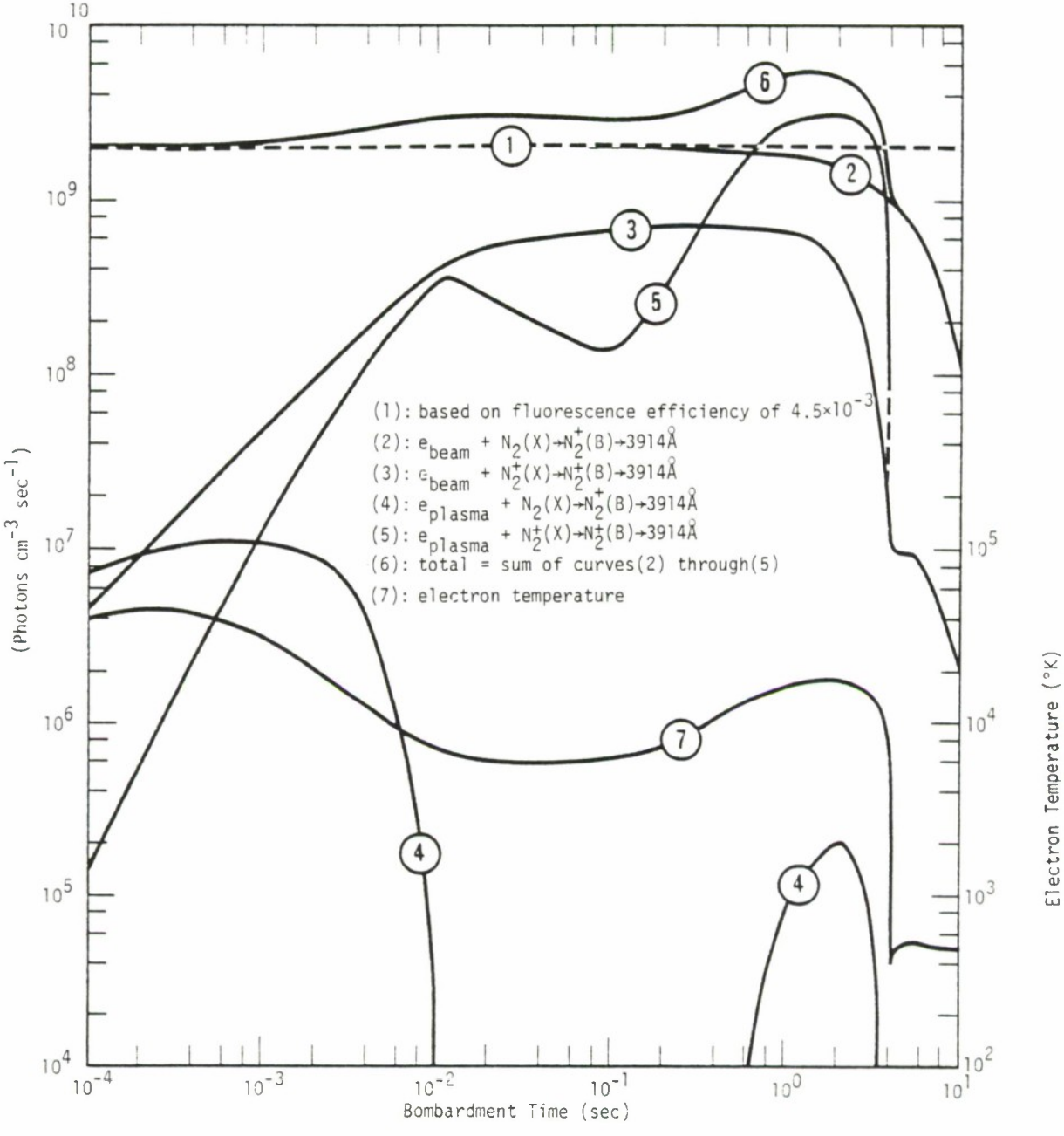

Figure 2-9. Calculated 3914Å volume emission rate at 123-km altitude for an energy deposition rate of 1.48×10^{12} eV cm^{-3} sec^{-1} by a 3 keV electron beam.

Therefore,

$$(\dot{\phi}_{3914})_{\text{beam on } N_2^+} \approx 1.6\ [N_2^+] \quad \text{(photons cm}^{-3}\ \text{sec}^{-1}\text{)} \qquad (2\text{-}8)$$

where, for $p(N(^2P))$, we have used the ARCTIC code value of 0.276.

A study of the curves in Figure 2-9 reveals the following. Until a time of 0.6 sec, the dominant emission mechanism is the direct ionization and excitation of N_2 by the beam electrons. For times between 0.6 sec and about 3.5 sec, however, the electron temperature, the electron density, and the N_2^+ concentration* are sufficiently large that plasma-electron excitation of N_2^+ is dominant. For times to about 0.3 sec, the second most important mechanism (based on our approximate treatment of it as outlined above) is excitation of N_2^+ ions by the beam electrons. At no time are the electron temperature and electron density simultaneously high enough for plasma-electron ionization and excitation of N_2 to be important. The total emission rate (curve 6) exceeds the nominal value (curve 1) by a factor of about 2.5 for bombardment times between about 1 and 2 sec, but after about 3.6 sec it is less than the nominal value because, by this time, the N_2 concentration* has decreased by dissociation.

Although, as mentioned above, the maximum increase in the 3914 Å emission rate beyond the nominal value is a factor of about 2.5, the increase during the actual bombardment time of an air parcel in the EXCEDE: SPECTRAL experiment (which is certainly less than about 0.1 sec because of rocket motion) is seen from Figure 2-9 to be no more than about 50 percent. This is a far cry from the 2 orders-of-magnitude or more increase required to account for the anomalous enhancement.

---

* See Figure 3-1 of Section 3.

The conclusion then is that, even for high-current beams, plasma heating by electrons that behave like independent particles is insufficient to raise the effective fluorescence efficiency at 3914 Å to the point where it can account for the observed EXCEDE:SPECTRAL data.

SOME BEAM PLASMA DISCHARGE CONSIDERATIONS

As mentioned earlier in this section, a likely candidate to explain the observed enhancement in the EXCEDE:SPECTRAL experiment is the beam plasma discharge (BPD) phenomenon that has been studied in the laboratory under both pulse (References 2-3, 2-4) and DC (References 2-5 and 2-6) conditions, and may have been observed in space during the Norwegian Polar 5 experiment (Reference 2-17). In this subsection we briefly summarize some of the criteria that appear necessary for onset of a BPD, together with the observed optical consequences, and then attempt to determine the applicability of the phenomenon to nuclear burst, auroral, and EXCEDE environments.

Laboratory Observations and Inferences

The large vacuum tank experiments of Bernstein et al. can be interpreted (Reference 2-6) as defining a critical current, I_c, for onset of a BPD, for pressures $P < 2 \times 10^{-5}$ torr, by the expression

$$I_c \approx 10^{-10} \frac{V^{3/2}}{B^{0.7} PL} \quad \text{(amps)} \quad . \tag{2-9}$$

Here, V is the beam energy (volts), B is the magnetic field (gauss), and L is the system length (meters) which, in the Bernstein experiments was 20 m. Typically, for a 2 keV beam, I_c was found to have a value of about 40 ma which implies, for an effective beam diameter of 1 meter, a critical current density of about 5×10^{-6} amps cm^{-2}.*

---

* This value for the critical current density is also consistent with the critical beam electron density shown in Equation 2-14.

Alternatively, the Bernstein experiments (References 2-5, 2-6), run under DC-current conditions, and also the Getty and Smullin experiments (Reference 2-3), run under pulsed-current conditions, indicate that a necessary condition for BPD ignition occurs when the beam current produces a critical plasma density, N_{pe}, such that the plasma frequency, ω_{pe}, and the cyclotron frequency, ω_{ce}, are approximately equal. More recent experiments (Reference 2-4) give the threshold condition as $3.9 \leq \omega_{pe}/\omega_{ce} \leq 5.8$. This implies that

$$\left(\frac{4\pi N_{pe} e^2}{m}\right)^{1/2} \approx 5 \frac{eB}{mc} \qquad (2\text{-}10)$$

or,

$$N_{pe} \approx 25 \frac{B^2}{4\pi mc^2} \quad . \qquad (2\text{-}11)$$

For $B = 0.5$ gauss, Equation 2-11 yields the critical plasma electron density

$$N_{pe} \approx 6 \times 10^5 \ (cm^{-3}) \quad . \qquad (2\text{-}12)$$

On the other hand, Winckler (Reference 2-18) suggests that the discharge may occur when the Brillouin limit ($\omega_{be}^2 = 0.5\ \omega_{ce}^2$) is reached where ω_{be} refers to the beam itself. This would imply that the critical density of beam electrons, N_{be}, required for onset of the discharge is

$$N_{be} = \frac{B^2}{8\pi mc^2} \qquad (2\text{-}13)$$

or, for a field of 0.5 gauss,

$$N_{be} = 1.2 \times 10^4 \ (cm^{-3}) \quad . \qquad (2\text{-}14)$$

The optical consequences of a BPD, as measured in the Bernstein experiments (Reference 2-5), are that there is at least a 10 fold enhancement in the intensity of 3914 Å emission and an increase in the beam radius by a factor of 3. The phenomenon is also accompanied by strong radiowave emissions. However, these emissions will not be considered here since no instrumentation to detect them was present during the EXCEDE experiments.

Relevance to a Nuclear Environment

Electron energy deposition in a nuclear environment occurs mainly through X-ray photoelectrons and beta electrons from fission debris. Are either of these processes likely to induce a BPD condition? Consider each separately:

X Ray Absorption. In X-ray absorption, the photoelectrons are emitted preferentially at right angles to the direction of the incident X-ray photons, which move out radially from the burst point. Under such conditions, no electron beam is formed; consequently, no BPD can occur.

Beta-Particle Streamers. The current density of beta electrons can be estimated as follows. Let A be the area (km^2) over which radioactive debris is uniformly distributed. It can then be shown (Reference 2-19) that the number of betas, N_β, crossing unit area in unit time is given by

$$N_\beta = \frac{8.8 \times 10^{15} \, W_f}{A(1+t)^{1.15}} \quad (\text{betas cm}^{-2} \text{ sec}^{-1}) \qquad (2\text{-}15)$$

where W_f is the fission yield (MT), and t is the time (sec) after burst. The current density, J_β, is then

$$J_\beta = N_\beta / 6.25 \times 10^{18} \quad (\text{amps cm}^{-2}) \; . \qquad (2\text{-}16)$$

Furthermore, if v_β is the beta particle velocity, their number density is

$$n_\beta = N_\beta / v_\beta \; . \qquad (2\text{-}17)$$

For a circular distribution of debris over a radius R (km), the value of N_β, per MT of fission yield, at $t = 1$ sec, is

$$N_\beta(1) = \frac{1.26 \times 10^{15}}{R^2} \quad (\text{betas cm}^{-2} \text{ sec}^{-1} \text{ MT}^{-1}) \; . \qquad (2\text{-}18)$$

Equations 2-16, 2-17, and 2-18 then yield

$$J_\beta(1) = \frac{2.0 \times 10^{-4}}{R^2} \quad (\text{amps cm}^{-2}) \tag{2-19}$$

and, for 1.5 MeV beta particles with a velocity of 2.6×10^{10} cm sec^{-1},

$$n_\beta(1) = \frac{4.9 \times 10^{4}}{R^2} \quad (\text{cm}^{-3}) \quad . \tag{2-20}$$

Table 2-1 shows values of $n_\beta(1)$ and $J_\beta(1)$ for selected values of R.

Table 2-1. Beta particle concentration and current density per MT fission yield at 1 sec for 1.5 MeV betas.

Debris Radius (km)	$n_\beta(1)$ (electrons cm^{-3})	$J_\beta(1)$ (amps cm^{-2})
10	4.9×10^{2}	2×10^{-6}
10^2	4.9	2×10^{-8}
10^3	4.9×10^{-2}	2×10^{-10}
10^4	4.9×10^{-4}	2×10^{-12}

For high-altitude nuclear bursts involving fission yields as large as 1 MT, the debris radius is expected to exceed 100 km. Thus, from Table 2-1, we expect that in beta streamers $n_\beta < 5$ electrons cm^{-3} and $J_\beta < 2 \times 10^{-8}$ amps cm^{-2}. These values are to be compared with the corresponding values, suggested by laboratory data, and quoted in the previous subsection, of about 10^4 electrons cm^{-3} and 5×10^{-6} amps cm^{-2} for the minimum beam electron and current densities required for onset of a BPD. It thus appears that the

current density, or the beam electron density in beta streamers is much too low to induce any BPD effects.*

We conclude that the BPD phenomenon should not be present in a nuclear environment.

Relevance to the Aurora

Consider the case of an unusually strong class III aurora with a primary electron flux at the top of the atmosphere of the form

$$\Phi = 2.2 \times 10^{6} e^{-E_{keV}/8.5} \quad (\text{electrons cm}^{-2}\ \text{sec}^{-1}\ \text{eV}^{-1}) \quad . \quad (2\text{-}21)$$

This corresponds to an integrated deposition rate of 1.6×10^{14} eV cm^{-2} sec^{-1} that results in an auroral intensity at 3914 Å of about 230 kR.

It is easily shown that, for this strong aurora, the electron and current densities have the values of 6 cm^{-3} and 3×10^{-9} amps cm^{-2}, respectively. These numbers are clearly small compared with the corresponding values of 10^{4} cm^{-3} and 5×10^{-6} amps cm^{-2}, cited above, that appear to be required for onset of a BPD. We thus conclude that the BPD phenomenon is not present in an auroral environment.*

Relevance to EXCEDE Experiments

The average current density, J_b, and beam-electron density, N_{be}, for a beam radius R_b (cm), are given, respectively, by

$$J_b = \frac{I_b}{\pi R_b^{\,2}} \quad (\text{amps cm}^{-2}) \qquad (2\text{-}22)$$

---

* On the other hand, the minimum necessary plasma density requirement, stated by Equation 2-12, is easily satisfied in a beta patch or in a strong auroral arc. To our knowledge, no BPD effects have been observed in the aurora.

and

$$N_{be} = \frac{6.25 \times 10^{18} J_b}{v} \quad (cm^{-3}) \quad , \tag{2-23}$$

where I_b is the beam current (amps), and v is the velocity (cm sec^{-1}) of the beam electrons.

In the EXCEDE:SPECTRAL experiment, the nominal electron energy was 3 keV ($v=2.29\times10^9$ cm sec^{-1}), and the current was 7 amps per electron gun. Table 2-2 shows values in this case for J_b and N_{be}, inferred from Equations 2-22 and 2-23, for selected values of the beam radius.

Table 2-2. Average beam-electron and current densities in the EXCEDE:SPECTRAL experiment.

Beam Radius (m)	N_{be} (electrons cm^{-3})	J_b (amps cm^{-2})
1	6.1×10^5	2.2×10^{-4}
2	1.5×10^5	5.6×10^{-5}
3	6.8×10^4	2.5×10^{-5}
4	3.8×10^4	1.4×10^{-5}
5	2.4×10^4	8.9×10^{-6}

The effective beam radius, inferred from the onboard camera data (Reference 2-9), was about 2 m. For this radius, we see from Table 2-2 that the values for N_{be} and J_b exceed the corresponding critical values (of about 10^4 and 5×10^{-6}, respectively) for BPD onset by at least an order of magnitude. Furthermore, to the extent that it is relevant, the plasma density at 123-km altitude in EXCEDE:SPECTRAL builds up very rapidly to

values greatly exceeding the critical value of 6×10^5 given by Equation 2-12. Consequently, all of the criteria listed above for onset of a BPD seem to be well satisfied by EXCEDE electron beams.

In addition, the optical consequences of a BPD, as inferred from the Bernstein experiments, also seem to be satisfied, at least for the EXCEDE:SPECTRAL image we have studied. In particular, the laboratory-observed enhancement in the 3914 Å intensity by at least an order of magnitude is certainly well fulfilled by the EXCEDE results. Furthermore, the laboratory-observed increase in the beam radius by a factor of 3, after BPD onset, also appears to be duplicated in EXCEDE. This can be seen by comparing the dashed and upper solid curves in Figure 2-2. The upper solid curve is the calculated radial intensity distribution, increased by a factor of 10, and shifted to bring its peak into line with that of the dashed curve, which represents the measured radial distribution 4 meters in front of the electron gun. The full width at half maximum of the dashed curve is almost exactly a factor of 3 greater than that of the solid curve.

The conclusion then is, that the laboratory conditions for onset of a BPD, as well as certain optical properties of the resulting emission, appear to have been fulfilled in the EXCEDE:SPECTRAL experiment.

SECTION 3
UTILITY OF EXCEDE FOR PLASMA RADIATION VERIFICATION

PRELIMINARY

It has been established (Reference 1-1) that plasma radiation from the fireball plume of a high-altitude nuclear detonation is the single greatest potential source of interference with LWIR sensor systems. This radiation includes the continuum contribution resulting from free-free and free-bound collisions between electrons and ions, as well as line radiation from bound-bound transitions that occur following radiative-collisional recombination in an O^+/N^+ plasma. Although the formula used to describe the free-free+free-bound contribution is believed to be on solid theoretical ground, the models that describe the bound-bound radiation have not been adequately verified by the limited experiments (References 3-1, 3-2) performed.

Spectroscopic observations of the late-time Kingfish and Checkmate fireballs indicate that, during radiative-collisional recombination, many of the excited states of the neutral atoms from which photon emission arises are not in local thermodynamic equilibrium (LTE) with the ground state of the atom or of the parent ion (Reference 3-3). This means that the state populations cannot be determined simply from the Boltzmann Equation, or the Saha Equation, but rather from detailed non LTE calculations involving the rates for electron-ion recombination and for collisional and radiative cascade to the ground state of the atom. Many uncertainties are involved in these non LTE calculations; consequently, experimental verification of the results is highly desirable.

The experimental requirements for verification of the bound-bound radiation models, under non LTE conditions, have been reviewed by Sappenfield (Reference 3-3). The principal requirement is that the plasma density be reasonably high while, at the same time, the electron temperature be low. If both quantities are large, the excitation rate by collisions may be sufficiently great to assure LTE conditions which, for the experiment, we wish to avoid.

The question arises as to whether the requirements for verification might be met by an EXCEDE-type experiment. To help answer this question we made computer calculations using the ARCTIC code. The results of that study are reported in this section.

As explained in Section 2, the ARCTIC code was originally designed for use under auroral bombardment conditions that are about 10^6 times less intense than those encountered in EXCEDE experiments. As a consequence, considerable time and effort was required to modify the code so that it would be applicable under these extreme conditions, particularly with respect to a determination of the electron temperature. A brief outline of the modifications that were made in ARCTIC are given in Section 2, and a more detailed description can be found in Appendix A.

ARCTIC CODE CALCULATIONS

The calculations have been done for the case of EXCEDE:SPECTRAL, at altitudes of 90 and 123 km. In both cases we have assumed the maximum energy deposition rate, which occurs near the electron gun, as determined by our earlier code calculations. This rate, $\dot{\varepsilon}$, in normalized units for a single electron, is 1.97×10^3 eV gm^{-1} sec^{-1} $electron^{-1}$ (Reference 2-1, Figure 3-3). The deposition rate, $\dot{\mathscr{E}}$, in units of eV cm^{-3} sec^{-1}, is then given by

$$\dot{\mathscr{E}} = 6.25 \times 10^{18} \, I\rho\dot{\varepsilon} \quad , \tag{3-1}$$

where I is the beam current (amps), and ρ is the atmospheric density (gm cm^{-3}). For a 7 amp beam, the deposition rate is then

$$\dot{\mathscr{E}} = 8.62 \times 10^{22} \rho \quad . \tag{3-2}$$

Species Concentrations and the Electron Temperature

123-km Altitude. From Equation 3-2, with $\rho = 1.72 \times 10^{-11}$ gm cm^{-3}, the energy deposition rate input to the code is 1.48×10^{12} eV cm^{-3} sec^{-1}. The code was run for times from 10^{-7} sec to 10 sec. Some of the results are shown in Figure 3-1. Included are values for selected species concentrations as well as the electron temperature.

Some points to notice from Figure 3-1 are the following. The electron density builds up rather uniformly until about 10^{-1} sec when it begins to level off because it is approaching its quasi-equilibrium value ($\approx 1.5 \times 10^{9}$ cm^{-3}), controlled by dissociative recombination with the molecular ions, which tend to dominate the ion concentration until about 1 sec. However, dissociation of N_2 and O_2 by the continual electron bombardment results in a buildup in the N, N^+, O, and O^+ concentrations to the point where the ionization is dominated by the species N^+ and O^+ after about 1.5 sec. Recombination is then controlled by the slow radiative-collisonal process so that the electron density, along with the N^+ and the O^+ concentration, rises rapidly.

The electron temperature, T_e, first rises uniformly because the heating rate by the bombarding flux dominates the cooling rate from all processes until about 2.5×10^{-4} sec when T_e attains its maximum value of about 45,000 °K and the two rates are then equal. Subsequently, until about 10^{-1} sec, cooling by electronic and vibrational excitation of N_2 dominates the heating, and the temperature drops to about 6000 °K, a value too low to maintain significant excitation of the N_2. At this point, heating by the bombarding flux and by deexcitation of the metastable states of O^+,

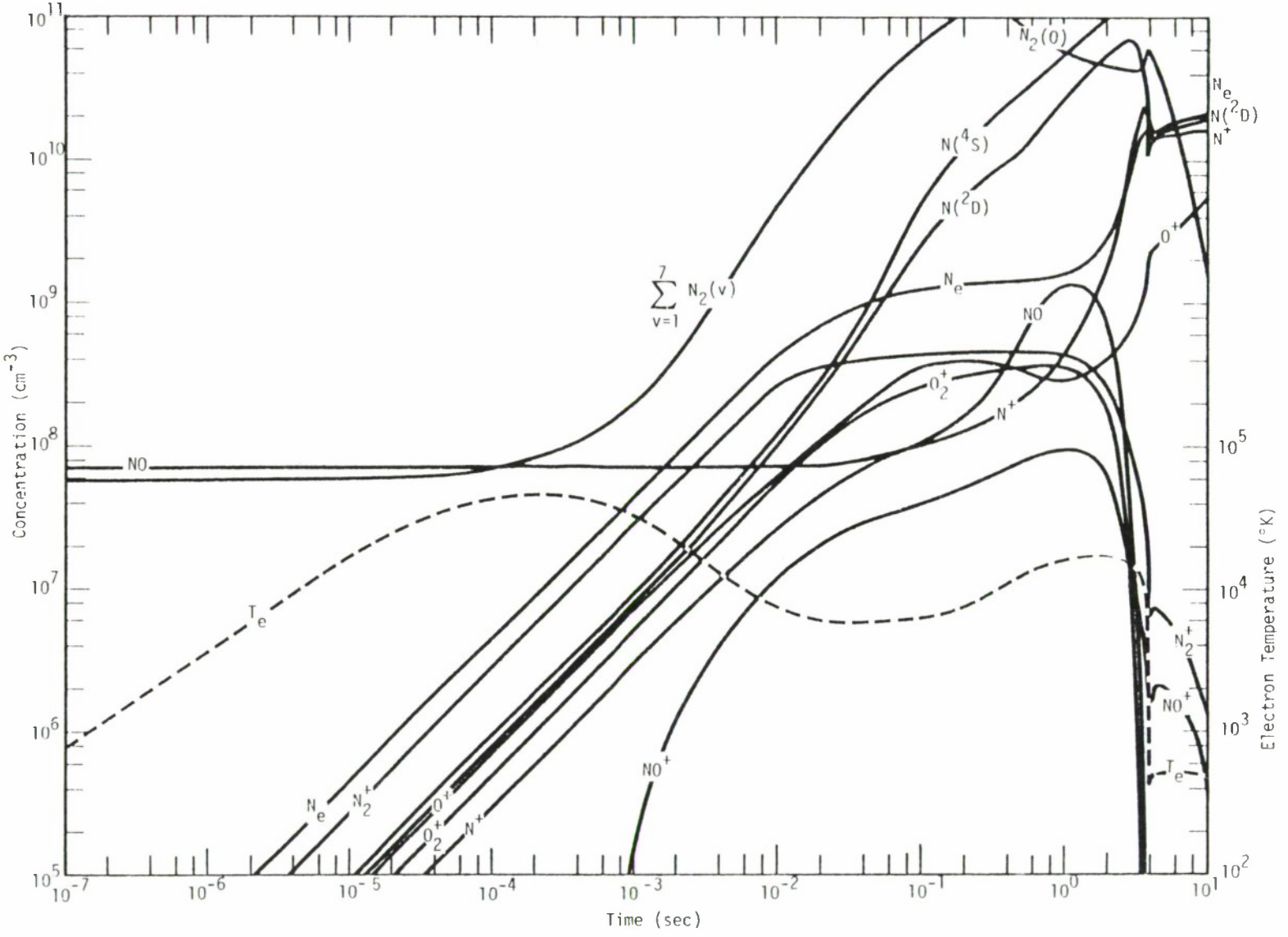

Figure 3-1. Calculated concentrations of selected species, and the electron temperature, at 123-km altitude under EXCEDE bombardment conditions. (Energy deposition rate = 1.48×10^{12} eV cm^{-3} sec^{-1}).

N^+, N and O dominates the cooling, and T_e then rises until about 2 sec when the heating and cooling rates are equal. However, the rapid rise in the atomic ion density after 1.5 sec produces a precipitously large rate of electron cooling by elastic collisions with the ions, and T_e drops rapidly from a value of about 10^4 °K at 3.6 sec to about 400 °K at 4 sec. Accompanying this drop in T_e is a corresponding increase in the value of the radiative-collisional recombination coefficient from 6.2×10^{-14} cm^3 sec^{-1} at 3.6 sec to 1.3×10^{-10} cm^3 sec^{-1} at 4 sec. This produces a sudden drop in the electron and ion densities, and thus in the electron cooling rate by elastic collisions with the ions, so that the electron temperature recovers somewhat and by 5 sec attains an equilibrium value of about 500 °K, while the electron density is close to its new equilibrium value of about 1.6×10^{10} cm^{-3}. By 10 sec, about 75 percent of the ions are N^+; the remainder are O^+.

90-km Altitude. From Equation 3-2, with $\rho = 3.4 \times 10^{-9}$ gm cm^{-3}, the energy deposition rate input to the code is 2.93×10^{14} eV cm^{-3} sec^{-1}. Results were obtained for times from 10^{-7} sec to 5.8 sec. Some of these, including values for selected species concentrations and the electron temperature, are shown in Figure 3-2.

The commentary on Figure 3-2 generally follows that for Figure 3-1. The electron density builds up rather uniformly until about 2×10^{-3} sec when it starts to level off and then attains its quasi-equilibrium value of about 1.2×10^{10} cm^{-3} which persists until about 1.5 sec. During this time the molecular ions N_2^+, O_2^+, and NO^+ are dominant so that the quasi-equilibrium electron density is controlled by dissociative recombination. However, dissociation of N_2 and O_2 by the bombarding flux results in a buildup in the N, N^+, O, and O^+ concentrations so that after 1.5 sec the ionization is dominated by N^+ and O^+ ions. Radiative-collisional recombination then takes over from dissociative recombination, and the electron density, along with the N^+ and the O^+ concentration, rises rapidly and by 5.8 sec the electron density attains a value of about 3×10^{11} cm^{-3}. The code was not pushed beyond 5.8 sec because of excessively long running times.

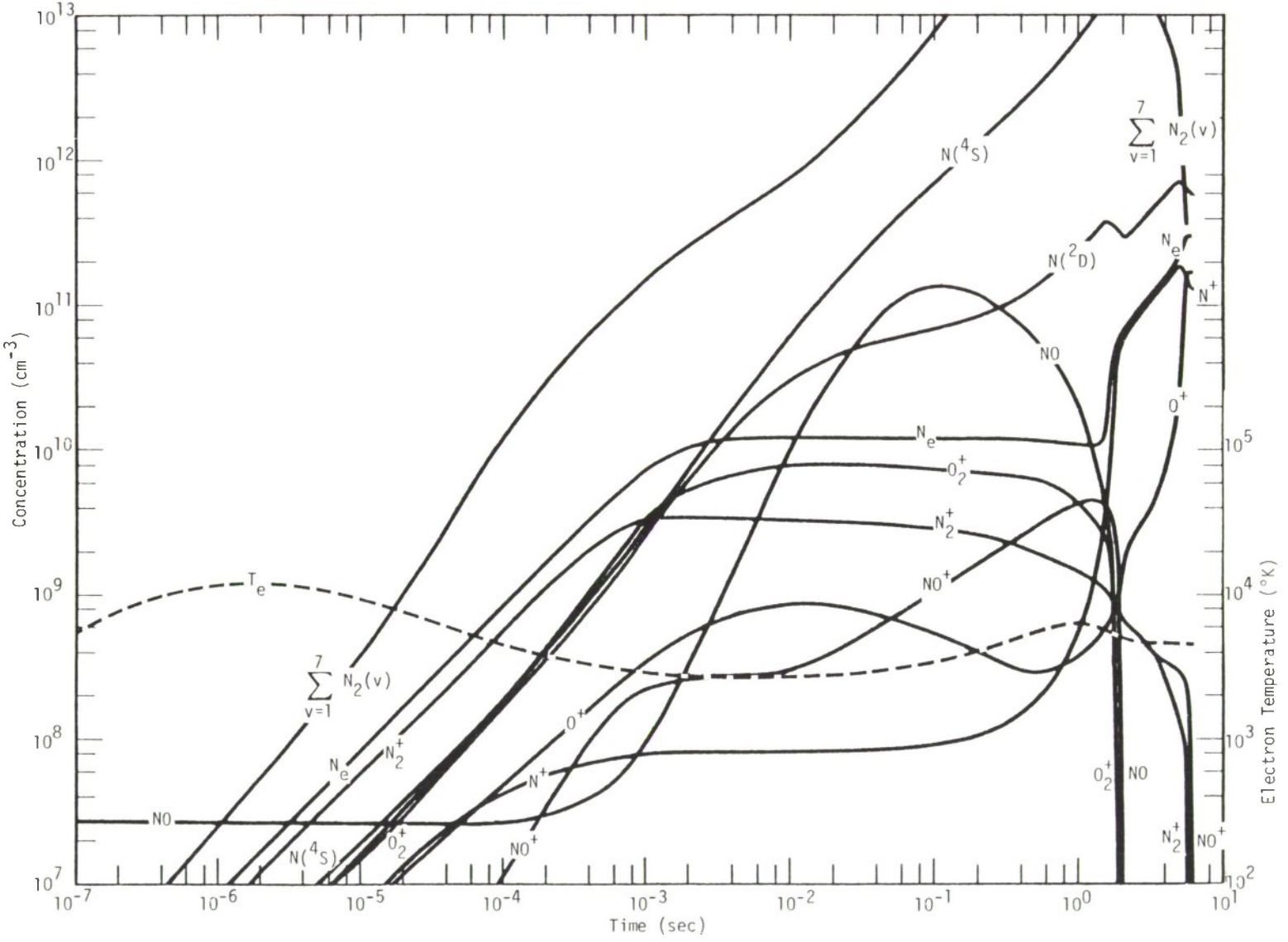

Figure 3-2. Calculated concentrations of selected species, and the electron temperature, at 90-km altitude under EXCEDE bombardment conditions. (Energy deposition rate = 2.93×10^{14} eV cm^{-3} sec^{-1})

Until about 1 sec, the electron temperature behavior is approximately similar to that described above in the 123-km case for times to 2 sec. From a value of about 6000°K at 1 sec, T_e then gradually subsides, mainly by excitation of $O(^1D)$ and $O(^1S)$ and fine structure excitation of $O(^3P)$, until about 2.5 sec when the equilibrium (or quasi equilibrium) temperature of about 4500°K is attained. The rapid drop in T_e seen above in the 123-km case has not occurred in this case, at least by 5.8 sec. This may be because the late-time cooling mechanisms are different in the two cases. At 123 km the electron cooling is mainly by elastic collisions with the ions; at 90 km, it is mainly by excitation of atomic oxygen.

Plasma Radiation

The volume emission rate from free-free (ff) + free-bound (fb) collisions of electrons with ions can be written as the frequency (ν)-independent expression (Reference 3-4)

$$J_\nu(\text{ff+fb}) = \frac{8\pi}{3\sqrt{6}} \left(\frac{g}{g_+}\right) \frac{e^6}{m^{3/2}c^3} \frac{N_+ N_e}{(kT_e)^{1/2}} \quad (\text{ergs cm}^{-3}\ \text{sec}^{-1}\ \text{ster}^{-1}\ \text{Hz}^{-1}) \quad . \tag{3-3}$$

Here, e and m are the electron charge and mass, respectively, N_e and N_+ are the electron and positive ion concentrations, respectively, T_e is the electron temperature (°K), k is Boltzmann's constant, and g/g_+ is the ratio of statistical weights of the ground states of the neutral and ion species. For hydrogen-like ions, which we assume here, $g/g_+ = 2$. Alternatively, with a change of units, Equation 3-3 becomes

$$J_\nu(\text{ff+fb}) = 5.39 \times 10^{-46} N_+ N_e T_e^{-1/2} \quad (\text{watts cm}^{-3}\ \text{ster}^{-1}\ \text{Hz}^{-1}) \tag{3-4}$$

or

$$J_{\lambda_\mu}(\text{ff+fb}) = 1.62 \times 10^{-31} \frac{N_+ N_e T_e^{-1/2}}{\lambda_\mu^2} \quad (\text{watts cm}^{-3}\ \text{ster}^{-1}\ \mu\text{m}^{-1}) \tag{3-5}$$

where λ_μ is the wavelength in micrometers.

For the volume emission rate from bound-bound (bb) transitions we have used the approximate expression (Reference 3-5)

$$J_{\lambda_\mu}(bb) = 2.65 \times 10^{-20} \frac{\alpha N_+ N_e}{T_e^{0.2145 \log_{10}\lambda_\mu} \lambda_\mu^{1.97}} \text{(watts cm}^{-3} \text{ ster}^{-1} \mu\text{m}^{-1}\text{)} \quad (3\text{-}6)$$

where α, the radiative-collisional recombination coefficient, is determined by

$$\alpha \approx 5.75 \times 10^{-13} N_e^{-0.1} \left(\frac{T_e}{11606}\right)^{[-0.0501(\log_{10}N_e)^2 + 0.4641 \log_{10}N_e - 1.913255]} \quad (3\text{-}7)$$

and T is the neutral termperature (°K). Although Equation 3-6 is a very low resolution approximation that does not describe the spikes associated with individual spectral lines, we believe that it is adequate for evaluating EXCEDE's utility as a plasma radiation experiment.

Equations 3-5 through 3-7 were used, together with values of $N_+([O^+]+[N^+])$, N_e, and T_e from Figures 3-1 and 3-2, to obtain plots of the quantity $\lambda_\mu^2 [J_{\lambda_\mu}(ff+fb)+J_{\lambda_\mu}(bb)]$. In these calculations, neutral temperatures of 175.0 and 367.3 °K were used for altitudes of 90 and 123 km, respectively. The results are shown in Figure 3-3.

For the 123-km case, the calculations show that the free-free+free-bound contribution exceeds the bound-bound contribution, for times to 3.8 sec, by factors that vary between about 1.6 and 5.6. However, for times after 3.8 sec, the bound-bound contribution is dominant by at least 2 orders-of-magnitude. This is because of the rapid drop in the electron temperature at this time that results in a large increase in the radiative-collisional recombination coefficient, as described above.

For the 90-km case, the bound-bound contribution exceeds the free-free+free-bound contribution at all times from about 10^{-4} sec to 5.8 sec

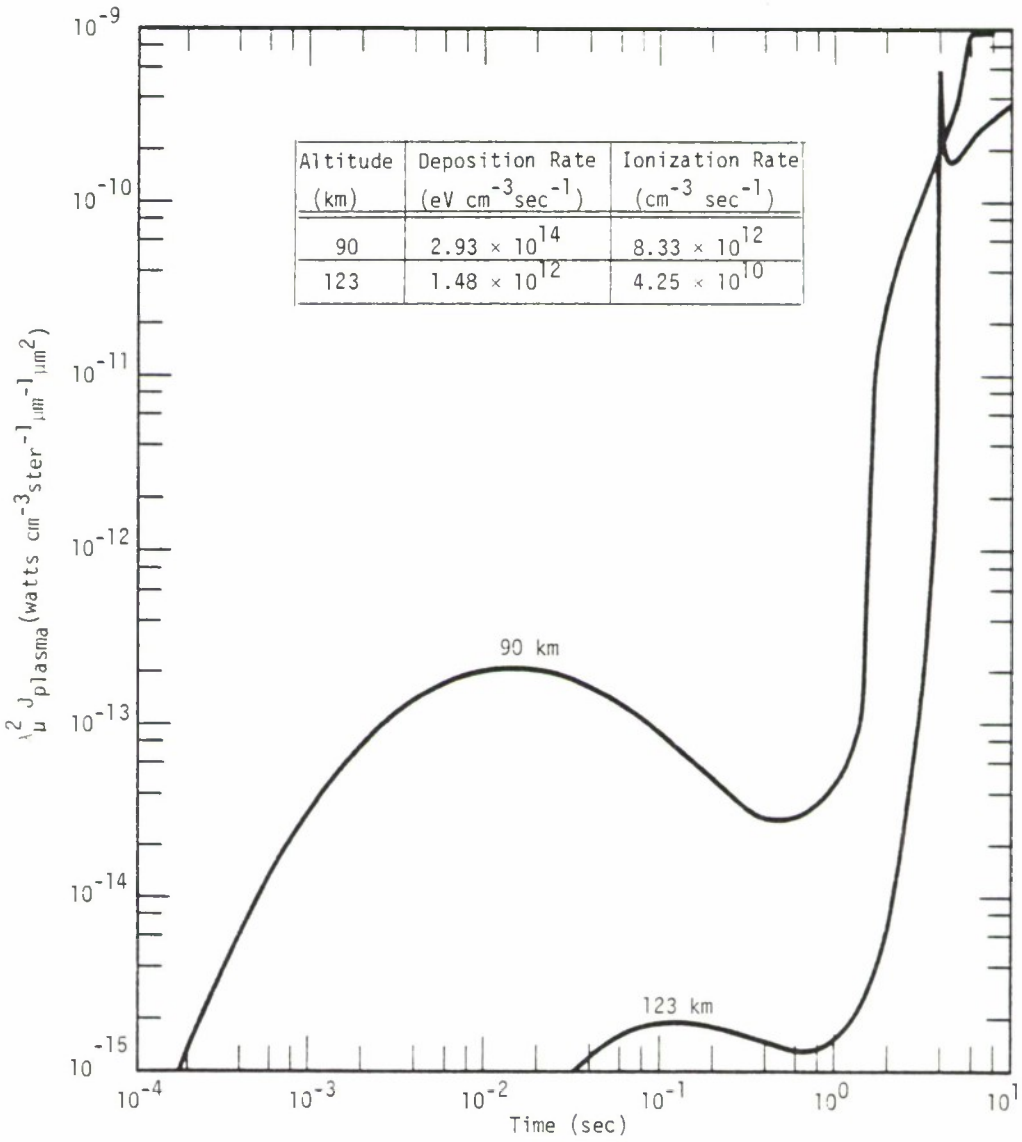

Figure 3-3. Calculated volume emission rate from plasma radiation (ff+fb+bb) at 90- and 123-km altitude in an EXCEDE-type experiment.

by factors that vary between about 1.2 and 4. At about 1.5 sec, the rapid rise in the electron density produces, by about 5.7 sec, a 4 order-of-magnitude increase in the plasma emission rate. However, because T_e is still fairly large, the bound-bound contribution at that time is only a factor of 4 larger than the free-free + free-bound contribution.

APPLICATION TO EXCEDE

As far as EXCEDE is concerned, the main point to note about both curves in Figure 3-3 is that the rapid increase in the emission rate does not occur until after one or more seconds of bombardment time. This is long compared with typical bombardment times in EXCEDE experiments that are usually limited to less than about 0.1 sec because of rocket motion. For bombardment times this short, it is clear from our calculations that not only is the magnitude of the plasma emission small, but also the bound-bound contribution, that we are especially interested in measuring, is either less than the free-free+free-bound continuum (123-km case) or is not significantly larger than it (90-km case).

To achieve bombardment times of a few seconds duration in an EXCEDE experiment would require flying the rocket parallel to the earth's magnetic field for a similar length of time. Although we are not familiar with the logistics involved in operating the rocket in this manner, we suspect that they are sufficiently difficult to render that mode of operation infeasible.

At this point we should emphasize that the foregoing results and considerations are based on our code calculations that assume the validity of the independent particle model in which the excitation and ionization is produced directly by the beam electrons. However, as discussed in Section 2, this model fails to account for the magnitude and dimensions of the intense

optical emission observed in the vicinity of the EXCEDE:SPECTRAL guns. It has been suggested that a BPD may, in fact, be responsible because the conditions for its ignition appear to have been satisfied in the EXCEDE experiments. If such is indeed the case, then the behavior of the plasma radiation, with respect to both its build-up time and its magnitude, may be quite different from that shown in Figure 3-3. For example, it has been observed that BPD's are ignited within a few microseconds after beam turn on and that plasma electrons, not beam electrons, are then the dominant ionization source (Reference 2-3). Under these conditions, one would expect a much earlier buildup in the plasma density and, possibly, in the intensity of plasma radiation.* The argument cited earlier against EXCEDE as a useful tool for performing a plasma radiation experiment, based on bombardment-time considerations, would then not be valid.

On the other hand, if BPD conditions in EXCEDE should "save the day" in terms of generating large bound-bound emission rates at early times, there would still be the problem of making accurate measurements of the electron temperature and atomic ion concentrations in the radiating region. It seems to us that an experiment of this nature could be done more readily, and probably less expensively, in the laboratory.

COMPETING MOLECULAR RADIATIONS

We have compared the magnitude of the calculated plasma radiation, integrated over the 8- to 12-μm and 2- to 5-μm bands, with competing molecular emission over the same wavelength regions. The results are shown below.

For the high deposition rates inherent in EXCEDE, we find that the IR molecular emission is completely dominated by N_2 fluorescence bands.

---

* However, if the effective electron temperature is very high under BPD conditions, because of internal electric-field heating, then the bound-bound plasma emission rate may, in fact, not be large.

An estimate of this fluorescence was made using some (unpublished) results obtained from the FLUOR code (RDA) and DANTE code (TEMPO) (Reference 3-6) in which we increased the Wu-Benesch contribution by a factor of 20 to conform with optical data from the EXCEDE:SPECTRAL experiment (Reference 3-7). Figures 3-4 and 3-5 show the resulting spectral efficiency, $\eta_{\tilde{\nu}}$, in units of ergs per cm^{-1} per 100 photons at 3914 Å, in the region from 200 to 5000 cm^{-1}, for altitudes of 92.5 and 120 km, respectively. The fraction, $f_{\Delta\tilde{\nu}}$, of the deposited energy that is radiated over the wavenumber interval $\tilde{\nu}_1$ to $\tilde{\nu}_2$ can be obtained from the relation

$$f_{\Delta\tilde{\nu}} = 8.9 \times 10^{6} \int_{\tilde{\nu}_1}^{\tilde{\nu}_2} \eta_{\tilde{\nu}} \, d\tilde{\nu} \quad . \tag{3-8}$$

From the previous subsection, the energy deposition rates assumed for altitudes of 90 and 123 km are 2.93×10^{14} and 1.48×10^{12} eV cm^{-3} sec^{-1}, respectively. These values, together with the fluorescence efficiency curves in Figures 3-4 and 3-5, lead to the volume emission rates for molecular radiation shown in Table 3-1. For both wavelength regions, the principal contributors are the Wu-Benesch ($W^3\Delta_u$-$B^3\Pi_g$) and First Positive ($B^3\Pi_g$-$A^3\Sigma_u^+$) band systems of N_2.

Table 3-1. Comparison between plasma and molecular radiation.

Altitude (km)	Wavelength Band (μm)	Volume Emission Rate (watts cm^{-3} $ster^{-1}$)	
		Molecular Radiation	Max. Plasma Radiation
90	2-5	1.1×10^{-8}	3.0×10^{-10}
	8-14	4.8×10^{-11}	5.4×10^{-11}
123	2-5	7.8×10^{-11}	1.2×10^{-10}
	8-14	3.8×10^{-13}	2.1×10^{-11}

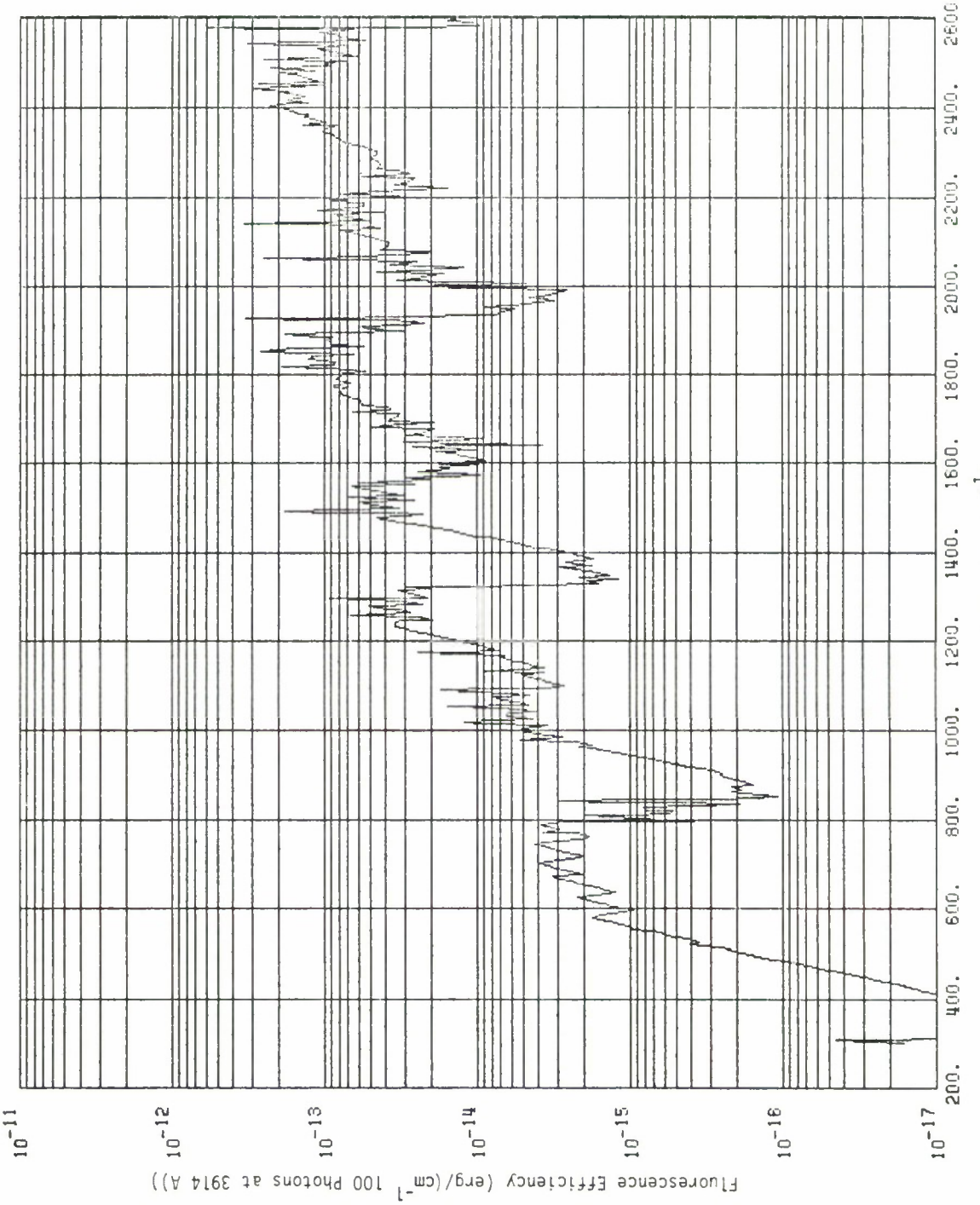

Figure 3-4a. N_2 fluorescence efficiency at 92.5 km (T = 192°K).

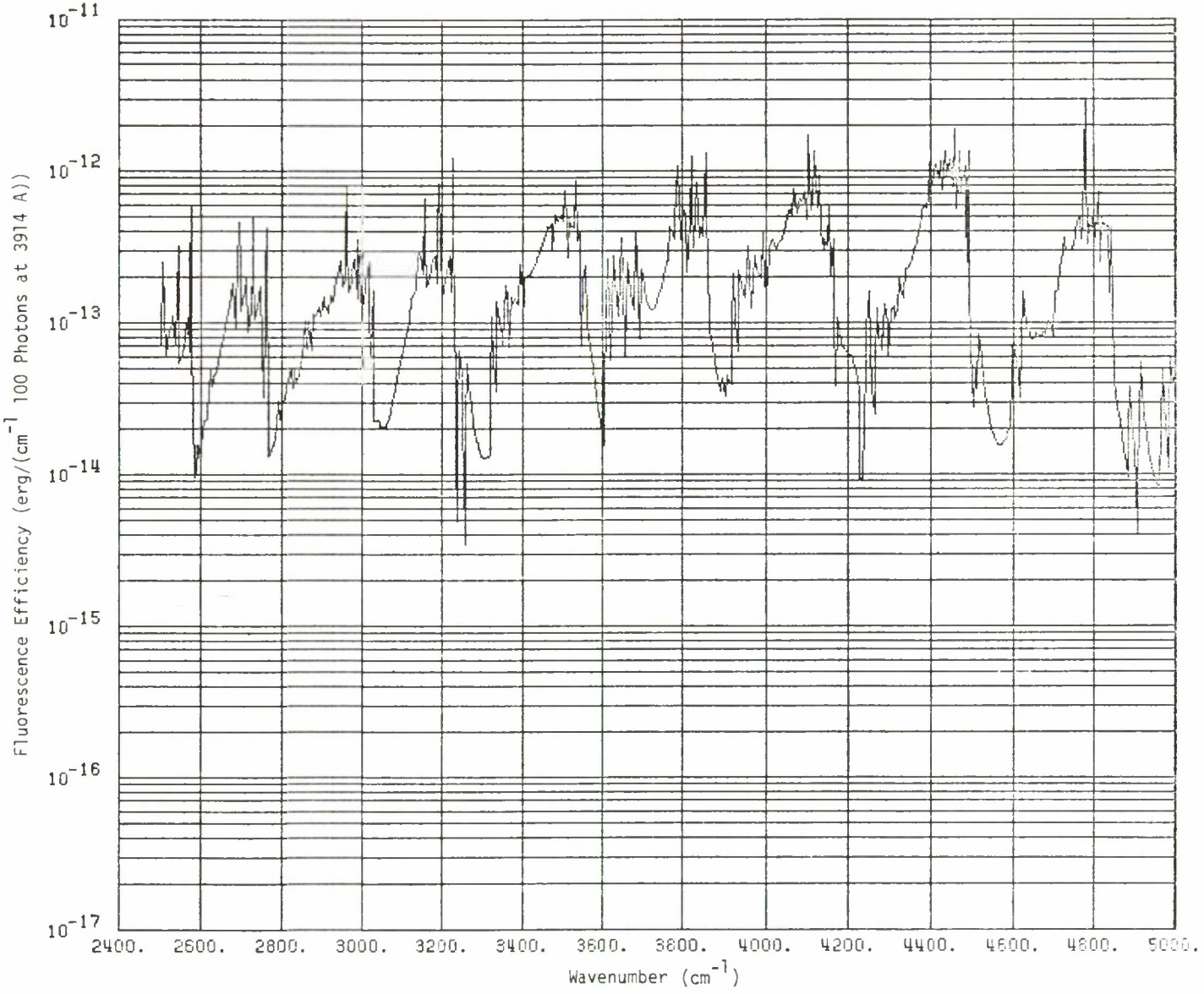

Figure 3-4b. N_2 fluorescence efficiency at 92.5 km (T = 192°K).

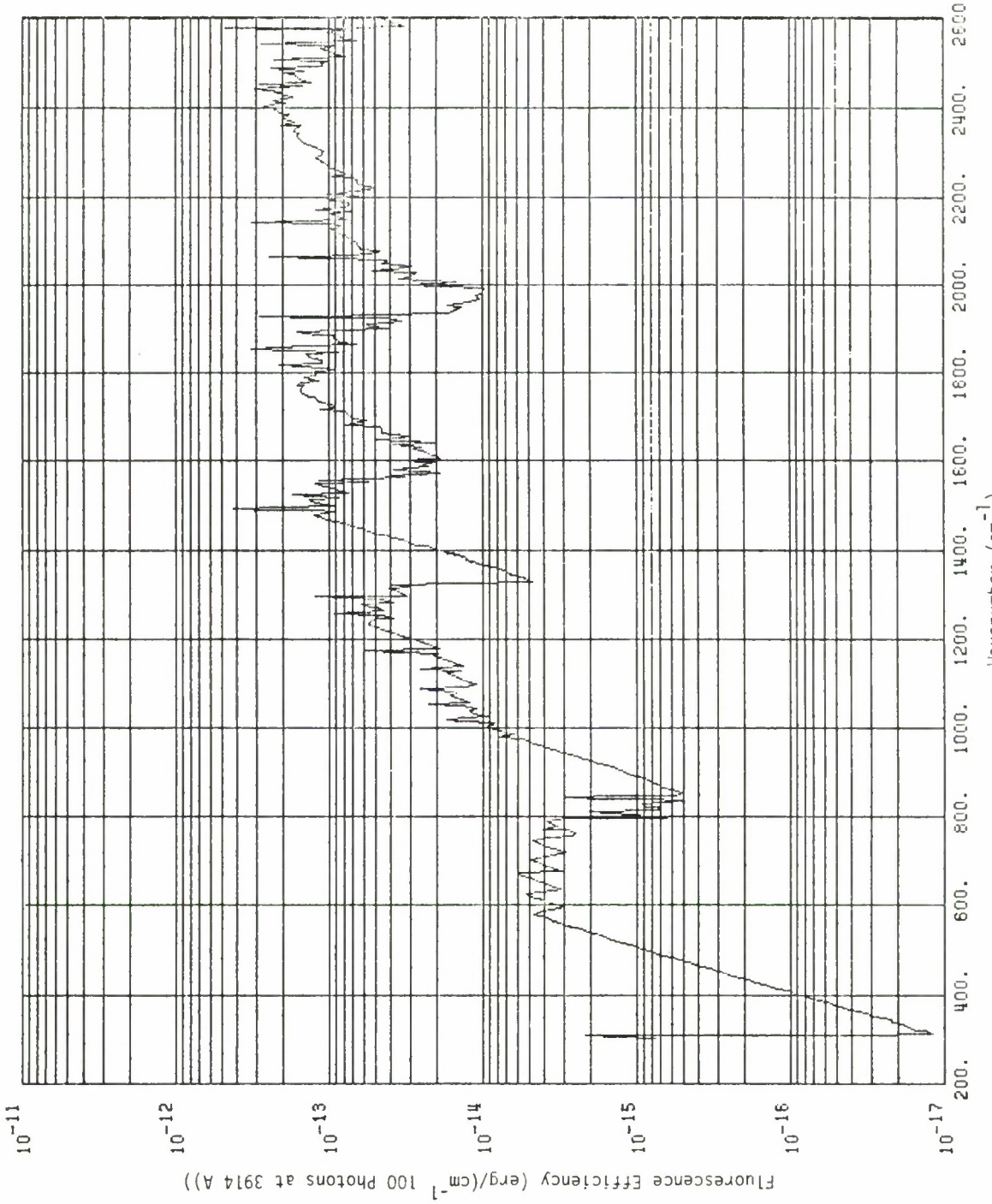

Figure 3-5a. N_2 fluorescence efficiency at 120-km altitude (T = 355°K).

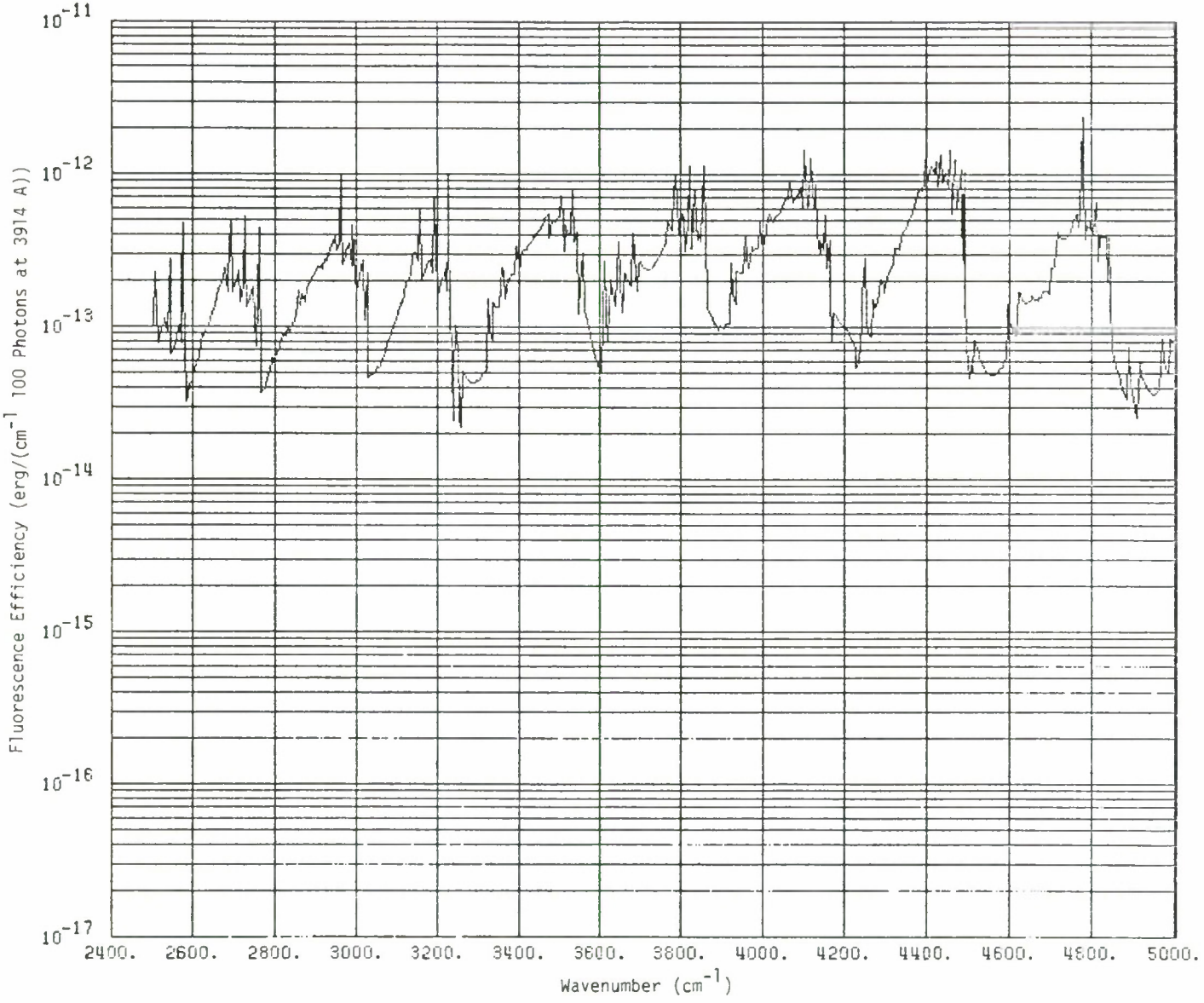

Figure 3-5b. N_2 fluorescence efficiency at 120-km altitude (T = 355°K).

To compare the molecular radiation with the corresponding plasma radiation, we note that since the latter varies approximately inversely as λ_μ^2 (Equations 3-5 and 3-6), the plasma emission, integrated between wavelengths λ_1 and λ_2, is

$$\int_{\lambda_1}^{\lambda_2} J_{\lambda_\mu} d\lambda_\mu = K \int_{\lambda_1}^{\lambda_2} \frac{d\lambda_\mu}{\lambda_\mu^2} = \left(\frac{1}{\lambda_1} - \frac{1}{\lambda_2} \right) K \qquad \text{(watts cm}^{-3}\text{ ster}^{-1}\text{)} \qquad (3\text{-}9)$$

where K is plotted in Figure 3-3. The maximum values of K shown in this figure are approximately 1×10^{-9} and 5×10^{-10} watts cm^{-3} $ster^{-1}$ μm^{-1} $(\mu m)^2$ for the 90-km and 123-km cases, respectively. Use of these values in Equation 3-9 then leads to the plasma emission rates shown in Table 3-1.

Points to note about the numbers shown in Table 3-1 are the following. In the 90-km case, it appears that the molecular emission dominates the plasma radiation over the 2-5 μm band, and that the two are nearly equal over the 8-14 μm band. In the 123-km case, the maximum plasma emission rate (almost exclusively from bound-bound radiation) exceeds the molecular emission by nearly 2 orders-of-magnitude in the LWIR band (8-12 μm), but by a much smaller factor in the SWIR band (2-5 μm). Thus, in the context of a plasma radiation experiment, the signal to noise ratio in the LWIR is significantly greater than it is at the shorter wavelengths.

In conclusion, it appears that molecular radiation, induced by electron-beam excitation of air, should not seriously interfere with observations of plasma radiation in the LWIR region at altitudes as high as 123 km once the plasma density has been built up sufficiently for electron-ion collisions to cool the plasma. However, this conclusion does not necessarily hold up under beam plasma discharge conditions, particularly if the internal electric fields should maintain a high value for the electron temperature

that would then serve to depress the radiative-collisional recombination coefficient and, hence, the bound-bound plasma emission rate. Furthermore, under such conditions, collisional excitation of radiation by the hot plasma electrons might well mask the recombination radiation.

SECTION 4
SOME LWIR CONSIDERATIONS

This section describes, very briefly, three LWIR-related topics that we considered as part of the work statement under the present contract. They are: (1) the possible excitation of LWIR emission from N_2O by solar pumping, (2) photon excitation of the LWIR bands of uranium- and fission-fragment oxide ions, and (3) preliminary assessment of how the relative importance of LWIR emission mechanisms, inferred from single-burst calculations, may be modified in a multiburst environment.

The need to consider Topics 1 and 2 was discussed in Reference 1-1 which treats the relative importance of various LWIR emission mechanisms in a single-burst environment. Our present work, as related to these two topics, has consisted primarily of literature surveys. Item 3 above is a natural outgrowth of the work reported in Reference 1-1. As yet, no in-depth study has been possible for a multiburst environment due to the very limited amount of calculational data available. This situation should be rectified in the near future when the optical/IR capability of the SCENARIO code is fully operative.

SOLAR PUMPING OF LWIR BANDS OF N_2O

The mechanism involved here is one in which a molecule is first electronically excited by UV- or visible-light absorption in its ground state. Subsequently, following radiative cascade, it may be left in a vibrationally excited state of the ground electronic state. If the

molecule is IR active, further radiative cascade will result in the emission of its characteristic IR bands.

It can be shown (Reference 4-1, p. 382) that the emission rate, $\dot{\varphi}_s$, of IR photons per molecule due to solar pumping is determined from the equation

$$\dot{\varphi}_s = \frac{\pi e^2}{mc} \eta \, \mathcal{F}_\nu f_e \quad . \tag{4-1}$$

Here, η is the number of IR photons emitted per visible/UV photon absorbed, $\mathcal{F}_\nu$ is the solar photon flux (photons cm^{-2} sec^{-1} Hz^{-1}), and f_e is the oscillator strength for the electronic transition involved. Clearly, two requirements for strong IR emission by this mechanism are: first, that there be strong absorption of visible or UV photons by the ground state into an upper state that can radiate back to the ground (electronic) state again (i.e. large f_e); second, that the solar flux, $\mathcal{F}_\nu$, be relatively large.

The first requirement precludes situations in which the absorption (strong though it may be) is to an upper state that spontaneously dissociates, or to one that overlaps a continuum so that predissociation (or preionization) may occur. The case of predissociation may result in diffuse visible/UV band radiation, but it is not likely to produce strong IR emission. The second requirement favors absorption by visible-light photons, rather than UV photons, because the solar flux varies approximately as λ^3. Thus, for example, other things being equal, absorption of 5500 Å photons will be about 60 times more effective in producing IR emission than will the absorption of 1400 Å photons.

We have surveyed the literature to determine the availability of suitable states of N_2O that may permit an effective solar-pumping mechanism to operate. The results are negative. In the first place, N_2O does not absorb in the visible spectral region (Reference 4-2). As for the UV region,

it is dominated by continuous absorption spectra, superimposed in certain spectral intervals by diffuse bands (Reference 4-3). Thus, qualitatively, the findings violate both criteria stated above for an effective solar-pumping mechanism.

Numerically, one may attempt to place an upper limit on the IR-photon emission rate by considering the measured total absorption cross sections for N_2O. For example, in the spectral region from about 1400 Å to 1600 Å the absorption spectrum consists of an apparent continuum on which are superimposed about 20 diffuse bands. A cross section peak of 8×10^{-18} cm^2 occurs at about 1450 Å (Reference 4-4). An integration of the published cross section then leads to a value for f_e of about 2×10^{-2}. Also, since $\mathscr{F}_\nu \approx 10$ at 1450 Å, Equation 4-1 yields, for $\dot{\varphi}_s/\eta$, a value of about 5×10^{-3}.

This number for $\dot{\varphi}_s/\eta$ is comparable to the corresponding numbers inferred for LWIR emission from N_2O excited by earthshine scatter (Reference 1-1, p. 84). However, since a major part of the UV absorption cross section appears to be attributable to the continuum, we must conclude that the actual value of $\dot{\varphi}_s/\eta$ for N_2O is much smaller than 5×10^{-3}. That is, we conclude that for N_2O the solar-pumping mechanism is much less effective in exciting the LWIR bands of N_2O than is the earthshine-scatter mechanism.

OSCILLATOR STRENGTHS FOR URANIUM- AND FISSION-FRAGMENT OXIDE IONS

In Reference 1-1 we concluded that, next to plasma radiation from plume regions of high-altitude bursts, the most important source of molecular radiation in a nuclear environment arises from uranium- and certain fission-fragment oxide ions. The uranium species involved are principally UO_2^+ and UO^+. Our estimate of their importance was based on assumed values for excitation of their IR bands by solar and earthshine radiation equal to

those for AlO.* This excitation depends on the magnitude of the electronic (for solar pumping) and vibrational (for earthshine scatter) oscillator strengths, or f numbers. The need to know the f numbers for the above-mentioned ions is clearly apparent in view of the potential these ions have for creating a structured LWIR nuclear environment that may degrade the performance of LWIR sensor systems.

With the hope of finding some experimental evidence relating to these f numbers, we conducted a search of the available literature. Not too surprisingly, no hard data were found.

Since that time, theoretical estimates have been reported (References 4-5, 4-6) for the vibrational f number of UO and UO^+. The upper-limit estimate of 5×10^{-5} for the fundamental bands of these species ($\lambda \approx 12$ μm) leads to a value of about 0.2 photons sec^{-1} $molecule^{-1}$, similar to the number assumed in Reference 1-1. Estimates have also been made of the solar pumping rate, $\dot{\varphi}_s$, (see Equation 4-1) in which values for η between 1 and 10 and values for f_e between 0.1 and 1 were assumed (Reference 4-7). These lead to numbers for $\dot{\varphi}_s$ ranging from about 2 to 200 IR photons sec^{-1} $molecule^{-1}$; numbers that are from 1 to 3 orders-of-magnitude larger than the value adopted in Reference 1-1. However, these values are purely speculative at the present time, being based on arguments related to the anticipated density of accessible electronic states. Firm numbers for the oscillator strengths, both vibrational and electronic, must await the results of successful laboratory experiments; hopefully, those currently being conducted at the Los Alamos National Laboratory (Reference 4-8).

---

* The calculated values for the 10.4-μm band of AlO, reported in Reference 1-1, are nearly the same for both solar pumping and for earthshine scatter — about 0.2 photons sec^{-1} $molecule^{-1}$.

MULTIBURST ENVIRONMENT

As mentioned earlier in this subsection, the conclusions reached in Reference 1-1 regarding the relative importance, or unimportance, of various LWIR emission processes in a high-altitude nuclear environment were based on calculations, and other considerations, for a single-burst situation. However, since a potential nuclear conflict is almost certain to involve multiple bursts, it behooves us to consider how the foregoing conclusions might be modified in a multiburst situation.

One of the conclusions reached, for example, is that LWIR emission from O_3 and CO_2 is not significantly enhanced above about 100-km altitude by a single megaton-class high-altitude burst. Is this conclusion still valid in a multiburst environment? To provide an adequate answer to this question, and a confirmation of the other conclusions, we need to perform multiburst calculations using a version of the SCENARIO code that incorporates an IR capability. Unfortunately, this version of SCENARIO, which is currently being developed at MRC, has not been available for our use under the present effort.

We have made a preliminary investigation, however, using the only IR-multiburst results available to us. These results were based on calculations performed at MRC a number of years ago, using the IRCHEM code, for a case in which two megaton-class bursts were detonated at two different high altitudes, separated in horizontal distance by 300 km, and in time by 60 sec. Unfortunately, the grid size outside the fireball region was quite coarse and so the spatial resolution in the regions where molecular emission might be important is very poor. With this in mind, we note that there is nothing in the calculational data for this case that would conflict with the conclusions reached in Reference 1-1. However, as emphasized above, more definitive conclusions must await the results anticipated from the SCENARIO code in the near future.

SECTION 5
SUMMARY AND CONCLUSIONS

This report addresses several topics related to EXCEDE experiments and, briefly, various items pertaining to LWIR emission in a nuclear environment. The following is a summary of the principal results and conclusions.

Regarding the spatial dimensions and mechanism involved in the anomalous region near the EXCEDE:SPECTRAL guns:

- A comparison between the calculated crosswise integrated intensity and that inferred from the ground-based photographic data shows that the enhanced optical emission from the pulse at 123-km altitude occurs in a region surrounding the accelerator that extends for several hundred meters along the magnetic field. A more accurate definition of the spatial extent of this enhanced region is not possible, for the EXCEDE:SPECTRAL experiment, because of the finite sensitivity of the photographic film.

- An attempt to salvage the independent particle model of energy deposition in EXCEDE experiments, by including excitation of 3914 Å radiation by hot plasma electrons, failed. During the bombardment time of a typical air parcel, the enhancement in the 3914 Å emission rate from this mechanism is at most about 50 percent. Thus, the independent particle model cannot account for the observed two order-of-magnitude enhancement in the optical emission rate. It appears likely that collective effects, producing internal electric fields that accelerate the plasma and beam electrons, are required to explain the observations.

- A somewhat cursory study of the beam plasma discharge phenomenon reveals that the criteria for its production, as well as the observed optical consequences, appear to be fulfilled in the EXCEDE:SPECTRAL experiment. Although this does not provide proof of the BPD mechanism in EXCEDE, the circumstantial evidence points strongly in that direction.

- Application of the laboratory-inferred criteria for onset of a BPD reveals that the phenomenon should not be present in either an auroral or a nuclear environment. This corroborates the assumption, implicit in auroral and nuclear models of electron energy deposition, that collective effects are not important. Therefore, the independent particle assumption, and the consequences therefrom, should be essentially valid in these cases.

Regarding the feasibility of utilizing EXCEDE as a tool for verifying our bound-bound models of IR plasma radiation:

- EXCEDE does not appear to be a useful tool in this respect.
  - If the excitation and ionization are produced primarily by the beam electrons themselves, then the bombardment time required (seconds) for adequate plasma-emission buildup exceeds the time available, in a typical EXCEDE experiment, by one to two orders of magnitude. Extending the bombardment time by flying the rocket parallel to the earth's magnetic field is probably not a viable option.
  - If BPD conditions exist, the time requirement should easily be fulfilled, but the electron temperature may remain high and severely depress the bound-bound plasma emission rate. In any event, accurate measurement of the electron temperature and the atomic ion densities would be required; measurements that are not likely to be performed easily or inexpensively in a space environment.

- Measurement of the bound-bound plasma radiation, originating from electron-beam irradiation of dry air for a sufficient period of time (under non-BPD conditions) should be relatively free from interference by competing molecular emissions, at least in the LWIR region. Whether or not this conclusion also holds under BPD conditions is presently unknown.

- Any electron beam experiment, designed to investigate bound-bound plasma radiation, is probably best carried out in the laboratory.

Regarding some LWIR considerations:

- Excitation of the infrared bands of N_2O by solar pumping should be small compared to that by earthshine scatter.

- As anticipated, available data are insufficient to render definitive conclusions regarding the magnitude of the f numbers for uranium oxide ions and, hence, on the magnitude of the LWIR emission therefrom.

- Preliminary investigations, based on very incomplete calculational data, suggest that the relative importance of various LWIR emission processes, inferred from single-burst calculations, may also be valid in a multiburst environment.

REFERENCES

1-1. Archer, D. H., Requirements for Improved Infrared Prediction Capability: LWIR, DNA 5471F, MRC-R-583, Mission Research Corporation, 31 October 1980.

2-1. Archer, D. H., EXCEDE Energy Deposition: Theory and Experiment Compared, DNA 5525F, MRC-R-599, Mission Research Corporation, 30 November 1980.

2-2. Omholt, A., The Optical Aurora, Springer-Verlag (1971).

2-3. Getty, W. D., and L. D. Smullin, "Beam-Plasma Discharge: Buildup of Oscillations," J. App. Phys. 34, 3421 (1963).

2-4. Szuszczewicz, E. P., et al., Threshold Criteria for a Space-Simulation Beam-Plasma-Discharge, NRL Memorandum Report 4608, Naval Research Laboratory, Washington, D.C., 23 September 1981.

2-5. Bernstein, W., et al., "Electron Beam Injection Experiments: The Beam-Plasma Discharge at Low Pressures and Magnetic Field Strengths," Geophys. Res. Lett. 5, 127 (1978).

2-6. Bernstein, W., et al., "Further Laboratory Measurements of the Beam-Plasma Discharge," J. Geophys. Res. 84, 7271 (1979).

2-7. Jost, R. J., et al., "Electron Energy Distributions Measured During Electron Beam/Plasma Interactions," Geophys. Res. Lett. 7, 509 (1980).

2-8. Boquist, W. P., Technology International Corporation, Private Communication, July 1981.

2-9. Sluder, R. B., and I. L. Kofsky, "EXCEDE SPECTRAL: Rocketborne Photographic Measurements," from "EXCEDE SPECTRAL Preliminary Results, AFGL-TM-41, Air Force Geophysics Laboratory, R. R. O'Neil (Ed.), 1980.

2-10. Kofsky, I. L., Photometrics, Inc., Private Communication, October 1980.

2-11. Boquist, W. P., Technology International Corporation, Private Communication, February 1981.

2-12. Crandall, D. H., et al., "Absolute Cross Sections for Electron-Impact Excitation of N_2^+," Phys. Rev. A9, 2545 (1974).

2-13. Tarr, P. W., et al., Studies of Auroral Simulation, DNA 3297F, MRC-R-122, Mission Research Corporation, 11 April 1974.

2-14. Archer, D. H., and P. W. Tarr, Auroral Simulation Studies, DNA 3567T, MRC-R-152, HAES Report No. 6, Mission Research Corporation, 22 April 1975.

2-15. Tarr, P. W., Arctic Code Electron Deposition Theory with Application to Project EXCEDE, DNA 3636T, MRC-R-173, HAES Report No. 10, Mission Research Corporation, 18 June 1975.

2-16. Archer, D. H., and P. W. Tarr, Final Report on Auroral Simulation Effects, DNA 4275F, MRC-R-313, HAES Report No. 62, Mission Research Corporation, 31 March 1977.

2-17. Grandal, B., et al., The Polar 5 Experiment: Measurements of the 391.4 nm. Light Produced by an Artifical Electron Beam in the Upper Atmosphere, Intern Rep. E-286, Norw. Def. Res. Estab., Kjeller, Norway, 1978.

2-18. Winckler, J. R., "The Application of Artificial Electron Beams to Magnetospheric Research," Rev. Geophs. and Space Phys. 18, 659 (1980).

2-19. Knapp, W. S., and P. G. Fischer, Aids for the Study of Electromagnetic Blackout, DASA 2499, July 1970.

3-1. Hymann, H., et al., Plasma Radiation Effects, DNA 3554F, February 1975.

3-2. Jones, L. A., Bound-Bound Radiation/Collisional-Radiative Recombination in Oxygen and Nitrogen Plasmas, DNA 3565F, February 1975.

3-3. Sappenfield, D. S., Mission Research Corporation, Private Communication.

3-4. Zel'dovich, Ya. B., and Yu. P. Raizer, Physics of Shock Waves and High Temperature Hydrodynamic Phenomena, Academic Press, New York, 1966.

3-5. Sappenfield, D. S., Radiation from a Recombining Oxygen Plasma, Los Alamos Scientific Laboratory, LA-4303, Supplement, April 1971.

3-6. Stephens, T. L., G.E. TEMPO, Private Communication, March 1979.

3-7. O'Neil, Robert R., Proceedings of the DNA Infrared Program Meeting, 23-24 January 1980, Washington, D.C.

4-1. Archer, D. H., in Physics of High-Altitude Nuclear Burst Effects, Ch. 7, DNA 4501F, MRC-R-30, Mission Research Corporation, December 1977.

4-2. Herzberg, G., Electronic Spectra and Electronic Structure of Polyatomic Molecules, Van Nostrand (1966).

4-3. Hudson, R. D., Critical Review of Ultraviolet Photoabsorption Cross Sections for Molecules of Astrophysical and Aeronomic Interest, NSRDS-NBS 38, Joint Institute for Laboratory Astrophysics, and National Bureau of Standards, August 1971.

4-4. Zelikoff, M., et al., "Absorption Coefficients of Gas in the Vacuum Ultraviolet, II Nitrous Oxide," J. Chem. Phys., 21, 1643 (1953).

4-5. Michels, H. H., United Technologies Research Center, DNA Atmospheric Effects Meeting, Washington, D.C., 13-17 July 1981.

4-6. Krauss, M., National Bureau of Standards, ibid.

4-7. Armstrong, R. A., Air Force Geophysics Laboratory, Private Communication, September 1981.

4-8. Bieniewski, T. M., Los Alamos National Laboratory, DNA Atmospheric Effects Meeting, Washington, D.C., 3-17 July 1981.

APPENDIX A

ARCTIC-CODE MODIFICATIONS REQUIRED FOR INTENSE BOMBARDMENT CONDITIONS

PRELIMINARY

A description of the ARCTIC code, as written for use under auroral simulation conditions, has been given in References 2-13 through 2-16. One of the important quantities computed by the code is the electron temperature, T_e. It is determined from the basic equation

$$\frac{dT_e}{dt} = H - C \quad , \tag{A-1}$$

where H and C are, respectively, the heating and cooling rates per electron. The heating term arises mainly from the bombarding flux of electrons and, for auroral use, the cooling terms include electron energy loss by: (1) elastic collisions with N_2, O_2, O, and positive ions, (2) rotational excitation of N_2 and O_2, (3) fine structure excitation of $O(^3P)$, (4) vibrational excitation of N_2 and O_2, (5) excitation of $O(^1D)$ and $O(^1S)$ from $O(^3P)$, (6) excitation of $O^+(^2D)$ and $O^+(^2P)$ from $O^+(^4S)$, and (7) excitation of $N(^2D)$ and $N(^2P)$ from $N(^4S)$. Deexcitation of the above excited states by plasma electrons gives a negative contribution to the cooling rate which, in effect, adds to the electron heating rate.

The foregoing cooling mechanisms are entirely adequate for auroral conditions in which the electron temperature seldom exceeds about 3000 °K. However, under the intense bombardment conditions encountered in an EXCEDE experiment, the electron temperature can become sufficiently high, at least at early times after beam turn on, when the plasma density is still quite low,

to excite some of the higher-lying electronic states of the air atoms, molecules, and ions. Consequently, for an adequate representation of the electron temperature under such conditions, as well as for a determination of the (plasma) electron-impact excitation rate of 3914 Å emission, it is necessary to include these other states in the cooling process.

Furthermore, a review of the models in ARCTIC, valid for auroral applications, revealed that those for electron cooling by elastic collisions with N_2, O_2, O, and by vibrational excitation of N_2 and O_2, are not valid for large values of T_e. Consequently, it was necessary to revise them.

This appendix describes the additional cooling processes required, and presents analytical expressions for their rates together with revised rates for the other processes mentioned above. Also presented are the rates for 3914 Å emission and for ionization produced by hot plasma electrons.

REVISION OF ELECTRON COOLING RATES

Elastic Scattering by N_2, O_2, O

The cooling rate per electron due to elastic collisions with gas molecules can be written, in units of ergs electron^{-1} sec^{-1}, as (Reference A-1):

$$\left(\frac{dE}{dt}\right)_{elastic} = -\,4N\,\frac{mM}{(m+M)^2}\,k(T_e-T)\left(\frac{8k}{\pi}\right)^{1/2}\left(\frac{T_e}{m}+\frac{T}{M}\right)^{1/2}\langle\sigma^{(m)}\rangle \qquad (A\text{-}2)$$

where

$$\langle\sigma^{(m)}\rangle = K^3\int_0^\infty v^5\sigma^{(m)}(v)e^{-Kv^2}dv \qquad (A\text{-}3)$$

and

$$K = \left(\frac{2kT_e}{m}+\frac{2kT}{M}\right)^{-1} . \qquad (A\text{-}4)$$

Here, m and M are the masses of the electron and gas molecule, respectively, T is the neutral gas temperature, and $\sigma^{(m)}(v)$ is the momentum transfer cross section for electrons of velocity v in a gas of number density N.

We have approximated the momentum transfer cross sections with an expression of the form

$$\sigma^{m}(E) = \sigma_o(1+aE^{1/2})e^{-bE} \qquad (cm^2) \tag{A-5}$$

where E is the electron energy (eV). Alternatively,

$$\sigma^{(m)}(v) = \sigma_o(1+1.69\times10^{-8}av)e^{-2.8\times10^{-16}v^2} \quad . \tag{A-6}$$

Equations A-2 through A-6, together with the approximation

$$\frac{mM}{(m+M)^2} \approx \frac{m}{M} = \frac{5.48\times10^{-4}}{\mathcal{M}} \quad ,$$

where $\mathcal{M}$ is the molecular weight of the gas, lead to the cooling rate (eV electron^{-1} sec^{-1}):

$$\left(\frac{dE}{dt}\right)_{elastic} = -\,0.118\,\frac{\sigma_o N}{\mathcal{M}}\,T_e^{1/2}(T_e-T)(1+8.618\times10^{-5}bT_e)^{-3}\left(1 + 1.54\times10^{-2}\,a\sqrt{\frac{T_e}{1+8.61\times10^{-5}bT_e}}\right) \quad . \tag{A-7}$$

The cross sections, Equation A-5, have been fitted to data for N_2, O_2, and O; the fits being good for plasma electron energies up to about 10 eV. Values for the cross section parameters σ_o, a, and b, along with references to the data, are shown in Table A-1.

Table A-1. Parameters used in Equation A-5 to fit measured elastic scattering cross sections for N_2, O_2 and O.

Molecule	$\mathcal{M}$	σ_o (cm^2)	a ($eV^{-1/2}$)	b (eV^{-1})	References
N_2	28	1×10^{-16}	10.39	3.38×10^{-2}	A-2, A-3, A-4
O_2	32	3×10^{-17}	3.54	1.68×10^{-2}	A-3, A-5
O	16	7×10^{-17}	4.0	2.57×10^{-2}	A-3, A-6

Vibrational Excitation/Deexcitation of N_2

Involved here is the collection of reactions of the form

$$e + N_2(v) \longleftrightarrow e + N_2(v') \quad ; \quad v' > v \tag{A-8}$$

with forward and reverse rate coefficients $k_{vv'}$ and $k_{v'v}$, respectively. Thus, the net cooling rate per electron is

$$\left(\frac{dE}{dt}\right)_{N_2(vib.)} = \sum_{v,v'} \left\{k_{v'v}[N_2(v')] - k_{vv'}[N_2(v)]\right\} W_{v'v} \tag{A-9}$$

where $W_{v'v}$ is the energy difference between vibrational states v' and v.

Equation A-9 has always been an integral part of the electron temperature model in the ARCTIC code. However, the simplified rate coefficients used for auroral applications were found to be inapplicable at the high values for T_e encountered in EXCEDE experiments. Extensive modifications have, therefore, been made using the measured cross sections of Schultz (Reference A-7) and calculations by Chen (Reference A-8).

Since the vibrational excitation of N_2 for electron energies ≥ 1.6 eV proceeds through formation of temporary negative ion states, each cross section consists of a series of resonance peaks. In order to facilitate the analytical representation of each reaction rate coefficient, we have approximated the resonance peaks by a series of sawteeth. The rate coefficient for each forward reaction can then be expressed in the form

$$k_{v,v'} = \frac{7.2\times10^{-7}}{T_e^{1/2}} \sum_j \frac{\sigma_j}{\Delta E_j} \left\{ (E_j+\Delta E_j)^2 e^{a(E_j+\Delta E_j)} + (E_j-\Delta E_j)^2 e^{a(E_j-\Delta E_j)} - 2E_j^2 e^{aE_j} + \frac{2}{a^2}(2+aE_j)(aE_j-1)e^{aE_j} - \frac{[2+a(E_j+\Delta E_j)][a(E_j+\Delta E_j)-1]e^{a(E_j+\Delta E_j)}}{a^2} - \frac{[2+a(E_j-\Delta E_j)][a(E_j-\Delta E_j)-1]e^{a(E_j-\Delta E_j)}}{a^2} \right\} \qquad \text{(A-10)}$$

where

$$a = -1.16\times10^4/T_e \quad , \qquad \text{(A-11)}$$

and the summation is over the resonances for each of the excitation cross sections. Values of the parameters σ_j, E_j, and ΔE_j for each excitation reaction are shown in Table A-2.

Values for the inverse (deexcitation) rate coefficients can be obtained (using detailed balancing) from the equation

$$k_{v'v} = e^{W_{v'v}/kT_e} k_{vv'} \quad ; \quad v' > v \quad . \qquad \text{(A-12)}$$

From the known vibrational energy levels of N_2 (Reference A-9), we can substitute in Equation A-12 for $W_{v'v}$ and obtain the result

$$k_{v'v} = \exp\{3.38\times10^3(v'-v)[1-6.13\times10^{-3}(1+v+v')]/T_e\}k_{vv'} \qquad \text{(A-13)}$$

Table A-2. Values of parameters for use in Equation A-10.

$k_{vv'}$	σ_1	E_1	ΔE_1	σ_2	E_2	ΔE_2	σ_3	E_3	ΔE_3	σ_4	E_4	ΔE_4	σ_5	E_5	ΔE_5	σ_6	E_6	ΔE_6
$k_{0 \rightarrow 1}$	0.08	1.5	1.1	1.5	2.03	0.2	1.4	2.32	0.18	1.05	2.62	0.19	0.5	2.83	0.12	0.4	3.12	0.29
$k_{0 \rightarrow 2}$	1.1	2.08	0.25	1.0	2.44	0.18	0.56	2.75	0.15	0.32	3.0	0.18	0.12	3.31	0.38	0	0	1
$k_{0 \rightarrow 3}$	0.9	2.17	0.29	0.5	2.61	0.20	0.30	2.92	0.17	0.12	3.21	0.15	0	0	1	0	0	1
$k_{0 \rightarrow 4}$	0.8	2.25	0.29	0.4	2.72	0.15	0.16	3.04	0.19	0	0	1	0	0	1	0	0	1
$k_{0 \rightarrow 5}$	0.56	2.37	0.31	0.21	2.95	0.19	0.14	3.19	0.18	0	0	1	0	0	1	0	0	1
$k_{0 \rightarrow 6}$	0.51	2.54	0.3	0.17	3.00	0.22	0	0	1	0	0	1	0	0	1	0	0	1
$k_{0 \rightarrow 7}$	0.32	2.69	0.3	0.09	3.19	0.23	0	0	1	0	0	1	0	0	1	0	0	1
$k_{1 \rightarrow 2}$	0.25	1.54	0.6	3.0	1.71	0.2	0.3	2.46	0.2	0.3	2.78	0.25	0.25	3.0	0.18	0.18	3.23	0.2
$k_{1 \rightarrow 3}$	1.3	1.8	0.3	0.16	2.37	0.25	0.35	2.61	0.16	0.24	2.84	0.16	0.10	3.2	0.25	0.08	3.4	0.1
$k_{1 \rightarrow 4}$	0.5	1.86	0.3	0.2	2.4	0.25	0.21	2.6	0.22	0.16	2.85	0.15	0.09	3.2	0.14	0	0	1
$k_{1 \rightarrow 5}$	0.2	1.92	0.3	0.07	2.38	0.4	0.25	2.57	0.2	0.18	2.85	0.16	0.08	3.2	0.22	0	0	1
$k_{1 \rightarrow 6}$	0.05	1.95	0.15	0.15	2.36	0.23	0.16	2.63	0.12	0.15	2.78	0.12	0.15	3.0	0.15	0.08	3.3	0.15
$k_{1 \rightarrow 7}$	0.2	2.41	0.18	0.12	2.59	0.11	0.16	2.83	0.18	0.08	3.2	0.20	0.05	3.45	0.08	0	0	1
$k_{2 \rightarrow 3}$	0.15	1.26	0.35	1.6	1.42	0.17	0.4	1.58	0.19	0.5	2.0	0.22	0.2	3.03	0.8	0	0	1
$k_{2 \rightarrow 4}$	0.4	1.41	0.2	0.6	1.78	0.28	0.25	2.1	0.18	0.22	2.9	0.6	0	0	1	0	0	1
$k_{2 \rightarrow 5}$	0.8	1.85	0.2	0.1	2.18	0.3	0.18	3.0	0.6	0	0	1	0	0	1	0	0	1
$k_{2 \rightarrow 6}$	0.54	1.91	0.23	0.15	2.76	0.12	0.14	3.0	0.11	0.09	3.3	0.14	0.08	3.5	0.1	0	0	1
$k_{2 \rightarrow 7}$	0.23	1.92	0.15	0.23	2.08	0.15	0.15	3.05	0.6	0	0	1	0	0	1	0	0	1
$k_{3 \rightarrow 4}$	0.12	1.0	0.5	0.55	1.12	0.23	2.0	1.4	0.20	0.3	1.87	0.19	0.2	2.2	0.25	0	0	1
$k_{3 \rightarrow 5}$	1.0	1.46	0.25	0.4	2.3	0.35	0	0	1	0	0	1	0	0	1	0	0	1
$k_{3 \rightarrow 6}$	0.29	1.42	0.1	0.29	1.6	0.15	0.15	1.82	0.16	0.25	2.08	0.23	0.15	3.26	0.41	0	0	1
$k_{3 \rightarrow 7}$	0.1	1.58	0.23	0.22	1.85	0.15	0.12	2.04	0.11	0.12	2.25	0.15	0.08	2.89	0.08	0.09	3.38	0.53
$k_{4 \rightarrow 5}$	0.2	0.95	0.5	1.5	1.06	0.15	0.7	1.31	0.13	0.18	1.57	0.35	0.18	2.02	0.15	0.11	2.35	0.17
$k_{4 \rightarrow 6}$	0.4	1.03	0.17	0.71	1.28	0.15	0.69	1.43	0.14	0.15	1.77	0.15	0.31	2.1	0.16	0	0	1
$k_{4 \rightarrow 7}$	0.45	1.35	0.17	0.74	1.46	0.17	0.19	1.92	0.15	0.15	2.22	0.16	0	0	1	0	0	1

Vibrational Excitation of O_2

Using cross sections measured by Hake and Phelps (Reference A-5), we have computed the electron cooling rate (eV electron^{-1} sec^{-1}), valid to high values of T_e. The result is as follows:

$$\left(\frac{dE}{dt}\right)_{O_2(\text{vib.})} = -\frac{10^{-5}[O_2]}{T_e^{3/2}}\left(e^{-4700/T_e} + 2e^{-6875/T_e} + 2.3e^{-9050/T_e}\right.$$
$$+ 7.9e^{-11210/T_e} + 15.5e^{-13400/T_e} + 15.9e^{-15570/T_e}$$
$$\left. + 14.1e^{-17700/T_e} + 26.1e^{-20300/T_e}\right) \qquad \text{(A-14)}$$

The eight terms correspond, respectively, to contributions from excitation of the first eight vibrational levels

COOLING BY ELECTRONIC EXCITATION AND IONIZATION OF N_2, O_2, O

Table A-3 shows the additional electronic states of N_2, O_2, O, and their ions, along with their energies relative to the ground state of the neutral molecule, that we now consider as candidates for excitation by plasma electrons.* This subsection presents the analytical formulas that have now been incorporated into ARCTIC to calculate the plasma-electron cooling rates by excitation of these additional states.

Let k_{ij} be the rate coefficient for electron excitation of state j, at energy W_j, from the ground state of species i. Then the

---

* These states, among many others, have always been an integral part of the ARCTIC code insofar as their excitation by beam electrons is concerned.

Table A-3. Additional electronic states included in electron temperature calculation.

State	Energy (eV)	State	Energy (eV)	State	Energy (eV)
(1) $N_2(A^3\Sigma_u^+)$	6.2	(9) $N_2^+(D^2\Pi_g)$	22.0	(17) $O_2^+(A^2\Pi_u)$	16.9
(2) $N_2(B^3\Pi_g)$	7.4	(10) $N_2^+(C^2\Sigma_u^+)$	23.6	(18) $O_2^+(b^4\Sigma_g^-)$	18.2
(3) $N_2(C^3\Pi_u)$	11.0	(11) $O_2(a^1\Delta_g)$	1.0	(19) O_2^+(composite)	23.0
(4) $N_2(a^1\Pi_g)$	8.6	(12) $O_2(b^1\Sigma_g^+)$	1.64	(20) O(Rydberg)	9.2
(5) $N_2(b^1\Pi_u)$	12.8	(13) $O_2(A^3\Sigma_u^+)$	4.5	(21) O(Rydberg)	9.6
(6) $N_2^+(X^2\Sigma_g^+)$	15.6	(14) $O_2(8^3\Sigma_u^-)$	8.4	(22) $O^+(^4S)$	13.6
(7) $N_2^+(A^2\Pi_u)$	16.7	(15) $O_2^+(X^2\Pi_g)$	12.1	(23) $O^+(^2D)$	16.9
(8) $N_2^+(B^2\Sigma_u^+)$	18.75	(16) $O_2^+(a^4\Pi_u)$	16.1	(24) $O^+(^2P)$	18.5

cooling rate, per electron, due to excitation of species i, is

$$\left(\frac{dE}{dt}\right)_i = - [i] \sum_j k_{ij} W_j \quad , \tag{A-15}$$

where [i] is the concentration of species i. But the rate coefficient is given by

$$k_{ij} = \left\langle v\sigma_j^{(i)} \right\rangle = \sqrt{\frac{2}{m}} \int_{W_j}^{\infty} E^{1/2} \sigma_j^{(i)}(E) f(E) dE \quad , \tag{A-16}$$

where $\sigma_j^{(i)}(E)$ is the cross section for excitation of state j of species i by an electron of energy E, and f(E) is the electron energy distribution function.

For a Boltzmann distribution of electron energies,

$$f(E) = \frac{2\pi}{(\pi k T_e)^{3/2}} E^{1/2} e^{-E/kT} \quad , \tag{A-17}$$

and Equation A-16 can then be written, with E expressed in eV units, as

$$k_{ij} = \frac{8.36 \times 10^{13}}{T_e^{3/2}} \int_{W_j}^{\infty} E\sigma_j^{(i)}(E) e^{-bE/T_e} \, dE \qquad \text{(A-18)}$$

where the parameter b has the value 1.159×10^4. Equations A-15 and A-18 can now be combined to yield the following equation for the cooling rate (eV electron^{-1} sec^{-1}) by electronic excitation of species i:

$$\left(\frac{dE}{dt}\right)_i = - \frac{8.36 \times 10^{13}[i]}{T_e^{3/2}} \sum_j \int_{W_j}^{\infty} W_j \sigma_j^{(i)}(E) E e^{-bE/T_e} \, dE \quad . \qquad \text{(A-19)}$$

The cross sections employed in the ARCTIC code (Reference 2-13) for excitation of the states shown in Table A-3 have been used in Equation A-19 to obtain cooling rates for electronic excitation of N_2, O_2, and O. Included are states 1 through 10 in Table A-3 for N_2, states 11 through 19 for O_2, and states 20 through 24 for O. The integrals were then performed numerically, for selected values of T_e, and the results fitted with the following analytical expressions, each in units of eV electron^{-1} sec^{-1}.

$$\left(\frac{dE}{dt}\right)_{N_2(\text{electronic})} = -3.92 \times 10^{-6}[N_2]\exp\{-[6.04\times10^4/T_e + 0.16(\ell nT_e - 15.42)^2]\} \qquad \text{(A-20)}$$

$$\left(\frac{dE}{dt}\right)_{O_2(\text{electronic})} = -2.45 \times 10^{-6}[O_2]\exp\{-[1.662\times10^3/T_e^{0.6578} + 0.1528(\ell nT_e - 15.42)^2]\} \qquad \text{(A-21)}$$

$$\left(\frac{dE}{dt}\right)_{O(\text{electronic})} = -2.86 \times 10^{-6}[O]\exp\{-[2.437\times10^5/T_e^{1.086} + 0.17(\ell nT_e - 15.42)^2]\} \; . \qquad \text{(A-22)}$$

IONIZATION BY HOT PLASMA ELECTRONS

Excitation of states 6 through 10 in Table A-3 by plasma-electron impact on $N_2(X)$ produces additional ionization of N_2. Similarly, excitation of states 15 through 19 and states 22 through 24 produces additional ionization of O_2 and O, respectively. For example, the ionization rate of N_2 by the process

$$e + N_2(X) \rightarrow 2e + N_2^+ \qquad \text{(A-23)}$$

can be written as

$$\frac{dN_2^+}{dt} = k_{N_2^+} N_e [N_2] \quad , \qquad \text{(A-24)}$$

where $k_{N_2^+}$ is the rate coefficient for the process.

Equation A-18 has been used, together with the cross sections in the ARCTIC code for excitation of states 6 through 10, to obtain values for $k_{N_2^+}$ at selected values of T_e. The result has been fitted analytically and can be written, in units of $cm^3\ sec^{-1}$, as

$$k_{N_2^+} = 2.06 \times 10^{-7} \exp\{-[8.436 \times 10^5 / T_e^{1.167} + 0.16(\ell n T_e - 15.42)^2]\} \qquad \text{(A-25)}$$

Corresponding expressions for the ionization rate coefficients of O_2 and O, obtained in a similar manner, are as follows:

$$k_{O_2^+} = 1.35 \times 10^{-7} \exp\{-[2.643 \times 10^5 / T_e^{1.059} + 0.1528(\ell n T_e - 15.42)^2]\} \qquad \text{(A-26)}$$

$$k_{O^+} = 1.76 \times 10^{-7} \exp\{-[1.2 \times 10^6 / T_e^{1.225} + 0.17(\ell n T_e - 15.42)^2]\} \qquad \text{(A-27)}$$

Equations A-25 through A-27 have been incorporated into the ARCTIC code and provide additional ionization whenever T_e is sufficiently high.

PLASMA-EXCITATION OF N_2^+ FIRST NEGATIVE BANDS

In addition to excitation of the N_2^+ First Negative band system by a primary electron flux, excitation by plasma electrons may also contribute provided T_e is high enough. In particular, excitation may occur by impact on ground-state N_2 molecules:

$$e + N_2(X^1\Sigma_g^+) \rightarrow 2e + N_2^+(B^2\Sigma_u^+) \quad , \tag{A-28}$$

or by impact on ground-state N_2^+ ions:

$$e + N_2^+(X^2\Sigma_g^+) \rightarrow e + N_2^+(B^2\Sigma_u^+) \quad . \tag{A-29}$$

Equation A-18 has been used, with the ARCTIC-code cross section for process A-28, to compute values for the rate coefficient, k_{28}, at selected values of T_e. The result has been fitted analytically and can be written, in units of $cm^3\ sec^{-1}$, as

$$k_{28} = 2.55\times10^{-8}\exp\{-[4.83\times10^5/T_e{}^{1.095}+0.157(\ell nT_e-15.42)^2]\} \quad . \tag{A-30}$$

Similarly, using the cross section for process A-29 measured by Crandall, et al. (Reference A-10), we find

$$k_{29} = 2.66\times10^{-8}\exp\{-[7.1\times10^6/T_e{}^{1.757}+0.3408(\ell nT_e-11.513)^2]\} \quad . \tag{A-31}$$

It can be shown (Reference 2-13) that the volume emission rate of 3914 $\mathring{A}$ photons from the (0-0) band of the N_2^+ First Negative system is given by

$$\dot{\Phi}_{3914} \approx 0.65\ P[N_2^+(B)] \tag{A-32}$$

where $P[N_2^+(B)]$ is the production rate of the $B^2\Sigma_u^+$ state of N_2^+. Consequently, the volume emission rate of 3914 Å photons, excited by hot plasma electrons, is

$$\dot{\Phi}_{3914}^{(plasma)} = 0.65\ N_e(k_{28}[N_2] + k_{29}[N_2^+]) \quad . \tag{A-33}$$

Equations A-30 through A-33 have been incorporated into the ARCTIC code.

REFERENCES (APPENDIX A)

A-1. Takayanagi, K., and Y. Itikawa, "Elementary Processes Involving Electrons In the Ionosphere," Space Sci. Rev. 11, 380 (1970).

A-2. Engelhardt, A. G., et al., "Determination of Momentum Transfer and Inelastic Collision Cross Sections for Electrons in Nitrogen Using Transport Coefficients," Phys. Rev. 135, A1566 (1964).

A-3. Wedde, T., and T. G. Strand, "Scattering Cross Sections for 40 eV to 1 keV Electrons Colliding Elastically with Nigrogen and Oxygen," J. Phys. B: Atom. Molec. Phys. 7, 1091 (1974).

A-4. Finn, T. G., and J. P. Doering, "Elastic Scattering of 13 to 100 eV Electrons from N_2," J. Chem. Phys. 63, 4399 (1975).

A-5. Hake, R. D., and A. V. Phelps, "Momentum-Transfer and Inelastic-Collision Cross Sections for Electrons in O_2, CO, and CO_2," Phys. Rev. 158, 70 (1967).

A-6. Henry, R. J. W., "Elastic Scattering from Atomic Oxygen and Photodetachment from O^-," Phys. Rev. 162, 56 (1967).

A-7. Schultz, G. J., "Vibrational Excitation of N_2, CO, and H_2 by Electron Impact," Phys. Rev. 135, A988 (1964).

A-8. Chen, J. C. Y., "Theory of Subexcitation Electron Scattering by Molecules. II Excitation and Deexcitation of Molecular Vibration," J. Chem. Phys. 40, 3513 (1964).

A-9. Herzberg, G., Spectra of Diatomic Molecules, Van Nostrand (1950).

A-10. Crandall, D. H., et al., "Absolute Cross Sections for Electron-Impact Excitation of N_2^+," Phys. Rev. A9, 2545 (1974).

DISTRIBUTION LIST

DEPARTMENT OF DEFENSE

Defense Nuclear Agency
ATTN: NAFD
ATTN: NATD
ATTN: STNA
ATTN: RAEE
3 cy ATTN: RAAE
4 cy ATTN: TITL

Defense Technical Information Center
12 cy ATTN: DD

Undersecretary of Def for Rsch & Engrg
ATTN: Strat & Theater Nuc Forces, B. Stephan
ATTN: Strat & Space Sys (OS)

DEPARTMENT OF THE ARMY

Atmospheric Sciences Laboratory
ATTN: DELAS-EO, F. Niles

BMD Advanced Technology Center
ATTN: ATC-T, M. Capps
ATTN: ATC-O, W. Davies

BMD Systems Command
2 cy ATTN: BMDSC-HW

Harry Diamond Laboratories
ATTN: DELHD-NW-R, R. Williams, 22000
2 cy ATTN: DELHD-NW-P, 20240

US Army Foreign Science & Tech Ctr
ATTN: DRXST-SD

US Army Nuclear & Chemical Agency
ATTN: Library

USAMICOM
ATTN: DRSMI-YSO, J Gamble

DEPARTMENT OF THE NAVY

Joint Cruise Missiles Project Ofc
ATTN: JCMG-707

Naval Air Systems Command
ATTN: PMA 271

Naval Intelligence Support Ctr
ATTN: NISC-50

Naval Research Laboratory
ATTN: Code 4780, S. Ossakow
ATTN: Code 4720, J. Davis
ATTN: Code 7500, B. Wald
ATTN: Code 4780
ATTN: Code 6700
ATTN: Code 7950, J. Goodman
ATTN: Code 4700
ATTN: Code 4187

Naval Space Surveillance System
ATTN: J. Burton

DEPARTMENT OF THE NAVY (Continued)

Naval Surface Weapons Center
ATTN: Code F31

Office of Naval Research
ATTN: Code 412, W. Condell
ATTN: Code 414, G. Joiner

Strategic Systems Project Office
ATTN: NSP-2141
ATTN: NSP-43
ATTN: NSP-2722, F. Wimberly

DEPARTMENT OF THE AIR FORCE

Air Force Geophysics Laboratory
ATTN: OPR, H. Gardiner
ATTN: OPR-1
ATTN: LKB, K. Champion
ATTN: CA, A Stair
ATTN: R. O'Neil
ATTN: PHP
ATTN: PHI, J. Buchau
ATTN: R. Babcock

Air Force Weapons Laboratory
ATTN: NTYC
ATTN: SUL
ATTN: NTN

Air Force Wright Aeronautical Lab
ATTN: W. Hunt
ATTN: A. Johnson

Deputy Chief of Staff
Research, Development, & Acq
ATTN: AFRDSP
ATTN: AFRDS, Space Sys & C3 Dir
ATTN: AFRDSS

Foreign Technology Division
ATTN: TQTD, B. Ballard
ATTN: NIIS, Library

Rome Air Development Center
ATTN: OCS, V. Coyne
ATTN: TSLD

Rome Air Development Center
ATTN: EEP

Space Division
ATTN: YGJB, W. Mercer
ATTN: YKM, CPT Norton
ATTN: YKM, MAJ Alexander

OTHER GOVERNMENT AGENCIES

Institute for Telecommunications Sciences
National Telecommunications & Info Admin
ATTN: W. Utlaut
ATTN: L. Berry
ATTN: A. Jean

OTHER GOVERNMENT AGENCIES (Continued)

Central Intelligence Agency
ATTN: OSWR/NED
ATTN: OSWR/SSD, K. Feuerpfetl

Oepartment of Commerce
National Bureau of Standards
ATTN: Sec Ofc for R. Moore

Department of Commerce
National Oceanic & Atmospheric Admin
ATTN: R. Grubb

OEPARTMENT OF ENERGY CONTRACTORS

EG&G, Inc
ATTN: O. Wright
ATTN: J. Colvin

Lawrence Livermore National Lab
University of California
ATTN: L-31, R. Hager
ATTN: L-389, R. Ott
ATTN: Technical Info Dept Library

Los Alamos National Laboratory
ATTN: R. Jeffries
ATTN: J. Wolcott
ATTN: MS 670, J. Hopkins
ATTN: P. Keaton
ATTN: D. Simons
ATTN: MS 644, J. Zinn
ATTN: ESS-5, T. Kunkle
ATTN: C. Westervelt

Sandia National Lab
ATTN: D. Thornbrough
ATTN: D. Dahlgren
ATTN: T. Wright, Org 4231
ATTN: Space Project Div
ATTN: W. Brown, Org 1250
ATTN: 3141

Sandia National Labs, Livermore
ATTN: T. Cook
ATTN: B. Murphey

DEPARTMENT OF DEFENSE CONTRACTORS

Aerospace Corp
ATTN: D. Olsen
ATTN: I. Garfunkel
ATTN: J. Straus
ATTN: V. Josephson
ATTN: T. Salmi
ATTN: R. Slaughter

Berkeley Research Associates, Inc
ATTN: J. Workman
ATTN: S. Brecht
ATTN: C. Prettie

University of California at San Diego
ATTN: H. Booker

E-Systems, Inc
ATTN: R. Berezdivin

DEPARTMENT OF DEFENSE CONTRACTORS (Continued)

Charles Stark Draper Lab, Inc
ATTN: D. Cox
ATTN: J. Gilmore
ATTN: A. Tetewski

Comsat Labs
ATTN: O. Fang
ATTN: G. Hyde

Cornell University
ATTN: O. Farley Jr
ATTN: M. Kelly

ESL, Inc
ATTN: R. Heckman
ATTN: J. Lehman
ATTN: R. Ibaraki
ATTN: J. Marshall
ATTN: E. Tsui

General Electric Co
ATTN: A. Harcar

General Electric Co
ATTN: C. Zierdt
ATTN: A. Steinmayer

HSS, Inc
ATTN: D. Hansen

Institute for Defense Analyses
ATTN: H. Gates
ATTN: H. Wolfhard
ATTN: E. Bauer
ATTN: J. Aein

Johns Hopkins University
ATTN: J. Phillips
ATTN: T. Evans
ATTN: J. Newland
ATTN: P. Komiske

Kaman Sciences Corp
ATTN: T. Stephens

Kaman Tempo
ATTN: DASIAC
ATTN: W. Knapp
ATTN: W. McNamara

Lockheed Missiles & Space Co, Inc
ATTN: R. Sears
ATTN: J. Kumer

Lockheed Missiles & Space Co, Inc
ATTN: Dept 60-12

MIT Lincoln Lab
ATTN: D. Towle

McDonnell Douglas Corp
ATTN: H. Spitzer
ATTN: Technical Library Services
ATTN: R. Halprin
ATTN: W. Olson

DEPARTMENT OF DEFENSE CONTRACTORS (Continued)

Mission Research Corp
ATTN: R. Bogusch
ATTN: R. Hendrick
ATTN: R. Kilb
ATTN: S. Gutsche
ATTN: F. Fajen
6 cy ATTN: Tech Library
ATTN: F. Guigliano
4 cy ATTN: D. Archer

Physical Dynamics, Inc
ATTN: E. Fremouw

R&D Associates
ATTN: R. Lelevier
ATTN: R. Turco
ATTN: B. Gabbard
ATTN: F. Gilmore
ATTN: P. Haas

Science Applications, Inc
ATTN: C. Smith
ATTN: L. Linson
ATTN: E. Straker
ATTN: D. Hamlin

Science Applications, Inc
ATTN: SZ

Science Applications, Inc
ATTN: J. Cockayne

Technology International Corp
ATTN: W. Boquist

DEPARTMENT OF DEFENSE CONTRACTORS (Continued)

Pacific-Sierra Research Corp
ATTN: F. Thomas
ATTN: E. Field Jr
ATTN: H. Brode, Chairman SAGE

Pennsylvania State University
ATTN: Ionospheric Research Lab

Photometrics, Inc
4 cy ATTN: I. Kofsky

Physical Research, Inc
ATTN: R. Deliberis

SRI International
ATTN: J. Petrickes
ATTN: M. Baron
ATTN: G. Smith
ATTN: C. Rino
ATTN: W. Chesnut

Utah State University
ATTN: Sec Control Ofc for K. Baker
ATTN: Sec Control Ofc for L. Jensen
ATTN: Sec Control Ofc for D. Burt
ATTN: Sec Control Ofc for A. Steed

Visidyne, Inc
ATTN: J. Carpenter
ATTN: W. Reidy
ATTN: O. Shepard
ATTN: Humphrey